PHILOSOPHICAL TRANSACTIONS OF THE ROYAL SOCIETY A MATHEMATICAL, PHYSICAL & ENGINEERING SCIENCES

On Eddy Motions near Plates and Ducts, Induced by Water Waves and Periodic Flows

G. F. Knott and M. R. Mackley

Phil. Trans. R. Soc. Lond. A 1980 **294**, 599-623
doi: 10.1098/rsta.1980.0070

ON EDDY MOTIONS NEAR PLATES AND DUCTS, INDUCED BY WATER WAVES AND PERIODIC FLOWS

By G. F. KNOTT and M. R. MACKLEY
School of Engineering and Applied Sciences, University of Sussex, Falmer, Brighton, U.K.

(*Communicated by Sir James Lighthill, F.R.S.* – *Received* 22 *January* 1979 – *Revised* 19 *June* 1979)

[Plates 1–5]

CONTENTS

We report experimental observations on the nature of eddies formed at sharp edges by the action of periodic flows and the influence that these eddies might have on the efficient operation of certain types of wave energy converters.

Flow visualization techniques are employed to observe the interaction of regular gravity waves with immersed and semi-immersed flat plates. Similar techniques are applied to the example of a glass tube held vertically in a free surface. Here the special situation is examined when highly amplified flow-oscillations occur within the tube as a result of its particular resonant properties. It is found that the exit geometry is critical to the degree of eddy formation; when terminated with an abrupt exit, separation occurs both in the in-flow and the out-flow and a clearly defined succession of vortex rings is formed; when terminated with a flared bellmouth no such separation is observed and the flow remains well ordered through the cycle of oscillation. The energy losses associated with such flows are examined in detail, and from this the nature of the contribution from eddy formation is identified.

1. Introduction

Recent investigations concerning the extraction of energy from water waves have led to the development of several devices which are envisaged as operating in or beneath the surface of the ocean. Depending on their mode of operation these devices interfere to a greater or lesser extent with the wave orbital motions and experience in different ways the effects of periodic flows.

The observations reported in this paper concern the shedding of eddies in periodic flows and are of relevance to the efficient operation of wave energy devices, particularly those more recent examples which are either plate-like or which involve amplified flow through ducts. The findings are of equal importance to small and large scale operation alike, and can be related to the current testing of laboratory models.

The subject is not restricted to wave energy alone and has relevance to other areas of marine and hydraulic engineering and to aspects of the Natural Sciences where periodic flows are encountered. In most practical situations, including those treated here, the generation of eddies is detrimental to operation and must be minimized or avoided if possible. However, there do exist certain systems such as surge barriers and mixing devices which benefit from eddy motion, and for which a requirement exists to maximize their effect.

The detailed visual observation and recording of flows containing eddies can be traced back to classic drawings by Leonardo de Vinci (see, for example, Popham 1949). More recently Prandtl developed photographic techniques (Prandtl & Tietjens 1934), and many of his pictures of steady flows remain unequalled and appear in numerous current texts on fluid dynamics. Flow visualization techniques have been used extensively since then in the study of various eddy motions and the review by Werlé (1973) covers some of the many aspects investigated. Concerning periodic eddies, most attention appears to have been directed in two areas; namely the formation of Von Karmen vortex streets, (see, for example, Zdravkovich 1969), where an essentially periodic eddy stream is produced downstream of a stationary body subject to a steady or near steady upstream flow and, secondly, the flows associated with oscillating streamlined or bluff bodies in steady far-flows or stationary bodies in periodic flows.

Research in these latter subjects has been central to the understanding of fluid loading on structures in waves. Much of this has been concerned with deriving reliable working theories for predicting wave forces, either by the estimation of appropriate drag and inertia coefficients for substitution in Morrison's equation, or, for structures that are large in relation to wavelength, by the application of diffraction theory (see Hogben *et al.* (1977) for a recent summary of these techniques). A number of authors have paid particular attention to the case of periodic flows over bluff bodies in which separation and eddy motion occurs, since this represents the operating condition most critical to the survival of structural members in waves. Keulegan & Carpenter (1958) were among the first to make an extensive theoretical and experimental study of periodic flows past cylinders and plates. Their experimental technique was to generate a long standing wave across a tank, and to place horizontal cylinders and plates beneath the node in a region of the flow that was approximately uniform. By measuring the horizontal loading on the body and observing the mechanism of flow separation, they were able to relate the variation in force coefficients to a non-dimensional period parameter, and to examine the physical significance of the eddy shedding. Other experimental techniques have been employed to investigate similar phenomena. Isaacson & Maull (1976) subjected a vertical surface-piercing cylinder to regular waves, and also oscillated it transversely in still water. They gave a qualitative description of the

mechanism of flow separation, and estimated the transverse 'lift' forces induced by the eddies from measurements of pressure on the surface of the cylinder. Sarpkaya (1975) generated a uniform oscillating flow in a U-shaped duct and measured the forces on a cylinder and sphere suspended in the middle section.

In addition to the extensive experimental work on periodic flows past cylinders summarized above, some theoretical work has been done on potential flow models of vortex shedding. Stansby (1978) summarizes the current position, again with a clear emphasis on the loading on cylindrical structural members.

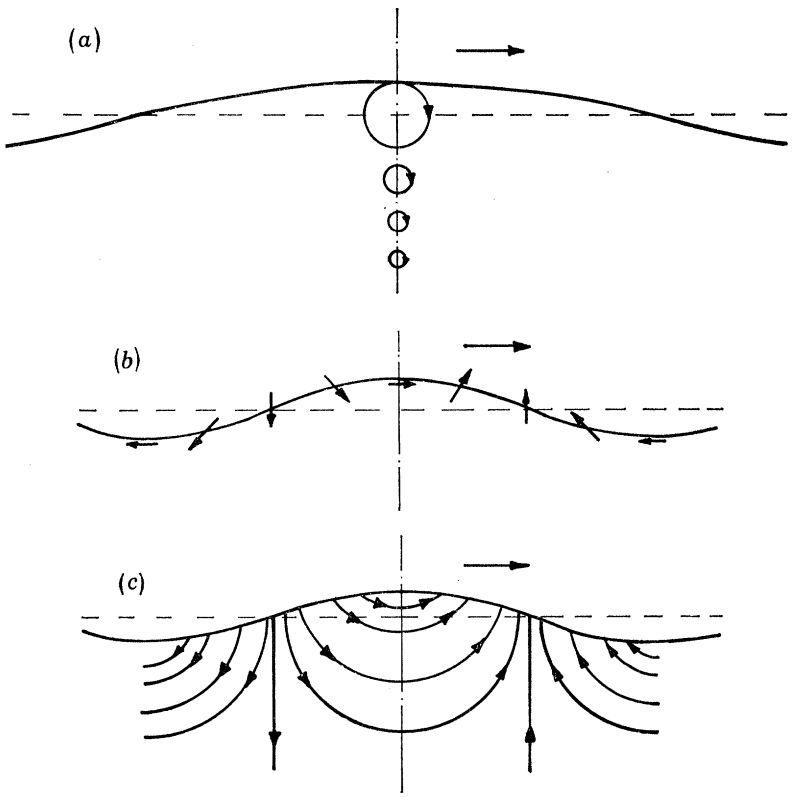

FIGURE 1. Schematic diagrams of orbital motion for harmonic, deep-water waves travelling from left to right, (*a*) the circular path of fluid particles, decaying exponentially with depth, as traced out during one wave period, (*b*) the direction of motion of fluid particles on the surface at an instant in time, and (*c*) the instantaneous streamlines beneath the surface.

We shall be dealing mainly with thin structures with sharp edges, which have received less attention to date, and with the periodic flow associated with progressive waves in deep water, which may be generally described as follows. For simple harmonic gravity waves travelling from left to right the fluid particles beneath the surface move in a clockwise, elliptical trajectory, returning almost to their point of origin at the end of each cycle, the difference being due to a small mean velocity in the direction of propagation (see, for example, Stoker 1957). In deep water the orbits are nearly circular, and their radii, r, decay exponentially with depth according to the relation

$$r = a\,e^{2\pi\zeta/\lambda},$$

where a is the wave amplitude, ζ is depth measured positive upwards and λ is the wavelength.

Figure 1 is a schematic representation of the idealized orbital decay, the instantaneous surface trajectories and the instantaneous streamlines of a progressive wave travelling from left to right. Naturally the introduction of a rigid body in the fluid will modify the flow field, leading to a reduction of local velocities at some points and a significant increase at others. Indeed, the introduction of sharp edges may lead to an increase in local velocities to well in excess of the maximum velocities in the freely-propagating wave, as has been observed for a wave propagating across an immersed sharp-edged duct (Knott & Flower 1979). In addition to such effects, fairly weak orbital motions may be amplified by the action of hydrodynamic resonance to levels which again greatly exceed their nominal values.

We begin our experimental observations by observing the interaction of waves with thin vertical two dimensional plates positioned normal to the direction of wave propagation. In one case the plate is fully submerged, extending downwards to the bottom of the tank, and attention is focused on the eddy formation that results from the periodic flow at its top edge. In the second case, the plate is half immersed, intersecting the free surface, the subject of interest being the eddy formation at the bottom edge. While such flows may be identified with any wave energy devices incorporating sharp edges, the most obvious candidates of interest are those devices that operate by means of flat vanes either in, or beneath the surface, of which there have been several variants (Leishman & Scobie 1976; Farley *et al.* 1978). When two such plates are placed parallel and close to one another, intersecting the free surface, the fluid between them is enclosed in a channel and is subject principally to vertical motion. This arrangement constitutes the crude basis for the 'air buoy' class of devices in which the oscillation of the fluid column, induced by the passage of waves beneath it, is damped by the control of the air pressure above it. This normally involves a turbine, operating in some form of air cavity. We have observed the case of the double plate, but do not include our findings here since there was little to distinguish the associated eddy motion from that of the single surface-piercing plate.

The oscillations of the fluid column between two essentially two dimensional plates rarely become large relative to the amplitude of the incident wave. As such, the nature of the flow differs little from that of a wave acting alone on a single plate. If the duct formed between the plates is made three 'dimensional', by enclosing the fluid column on all sides and setting the resulting duct in an 'infinite sea', the water column may resonate in response to waves with a greatly amplified motion. This situation is easily realized experimentally by using a vertical cylindrical duct. Resonant oscillations within ducts can be used to advantage in 'air buoys' floating in the surface, or in an ingenious variant, in a device, fully submerged beneath the surface, which contains its own 'atmosphere', such as is being currently developed by Vickers Ltd (see Lighthill 1979).

The experimental approach we adopt here is to observe by photographic techniques the fluid motions in and around a glass tube of circular cross section which is held vertically in the free surface of the water. Oscillation of the fluid column in response to continuous waves leads to an accumulation of complex eddies which tend to obscure the individual mechanism of eddy shedding. To avoid this and also to allow the fluid motion in the duct to be observed independently of wave action, we employed a method whereby motion was started from a state of rest by applying an impulsive force to the water column and allowing the resulting oscillation to continue and decay naturally. The end of the tube which was immersed in the water was terminated with two different geometries; in one case it was cut off abruptly, such that straight, parallel edges projected downwards into the tank and regular eddies were seen to be shed at the lips. In

the second, the mouth of the tube was flared into a 'bell-mouth' allowing a more ordered expansion of the flow and the virtual elimination of flow separation. From these tests and the results of a simple flow analysis, conclusions are drawn as to the nature and magnitude of flow losses induced by eddy formation.

2. Experiment and experimental procedure

Experiments were performed in a wave-tank illustrated schematically in figure 2. The tank is approximately 10 m long, 0.5 m wide and 0.9 m deep and is equipped with a servo-controlled wavemaker and a passive 'beach' to absorb unwanted reflexions.

Wave heights in the channel were measured by means of a non-contacting electromechanical gauge, as described in detail by Knott & Flower (1978), and the wave height within the tube was recorded by a 'twin-wire' resistance gauge consisting of two parallel surgical needles protruding down from an insulated terminal block.

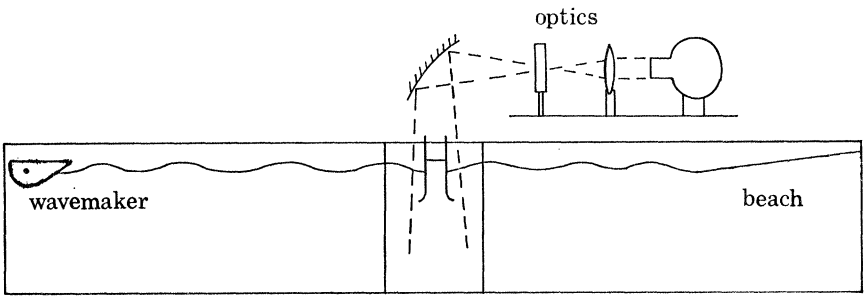

Figure 2. Schematic diagram of apparatus.

The working section was viewed through clear perspex side-walls, situated in the mid-section of the tank. Adjacent to this a small shrouded cubicle was constructed to house the camera and operator and allow photographs to be taken in an area of relative darkness, thereby reducing light interference from reflexions. Further extraneous sources of light were eliminated by shrouding the surface of the tank wherever possible and darkening the laboratory.

The optical system used to create the illumination appropriate for the photography is also illustrated in figure 2. This consisted of an intense source of light provided by a 150 W high pressure Hg lamp which projected onto a convex lens to produce a weakly divergent beam of light. This beam was focused in one plane by a cylindrical lens. The beam was reflected vertically downwards by a plane mirror, or pair of plane mirrors, and then passed through a 3 mm slit formed between two metal plates; this latter arrangement of mirrors and plates rested on a subframe across the tank.

For the purposes of visualization the water was seeded with fine polyethylene particles, which were distinguished for this particular application by being of near neutral buoyancy and of high reflective index. As a consequence of their brightness and the intense illumination of the source, a certain flexibility was possible with the choice of film and shutter speeds, allowing, for example, a fairly slow, fine-grain film to be used (Ilford FP4) at, typically, f8 and $\frac{1}{8}$ s. Still pictures were taken using a Contax 35 mm camera, augmented with an automatic motor drive unit, which permitted a rapid series of photographs to be taken in sequence (approximately 3 per second). An even faster, though less precise, series of pictures was taken on cine film with a 16 mm Bolex camera, from which additional qualitative information could be obtained.

Experiments with plates

In these experiments, designed to see how, in two dimensions, sharp edged obstructions interfere with oscillatory flows, a rigid steel plate, 3 mm thick, with its exposed edge forming a semicircle, was set in the tank, spanning the width and sealing with the walls at both ends. The plane beam of light was directed vertically downwards to illuminate the fluid equally on both sides as waves were directed along the channel. A proportion of the wave energy was reflected back, a proportion transmitted either over or under the plate and the remainder dissipated at the plate in eddies.

The reflecting particles were introduced into a restricted channel, about 5 cm wide, formed between the tank wall and a parallel sheet of perspex introduced into the water, This was necessary to limit the rate at which particles dispersed into the tank. The narrower channel thus formed against the side of the tank did not appear to inhibit the propagation of the wave or disturb the eddy shedding mechanism itself.

Experiments with surface-piercing tubes

Two glass tubes were used in these experiments one of which was uniform in cross section, having an internal diameter of 7 cm and external diameter of 7.6 cm; the other flared into a 'bell-mouth'. The shape of the 'flare' was arbitrarily chosen to be uniformly circular with a radius equal to the internal radius of the tube. These were attached vertically, by moveable clamps, to a framework that allowed their height relative to the water to be easily adjusted. Above the framework and in line with the centre of the tube, two plane mirrors were used to reflect the incident plane beam. Thus two coplanar, but mutually inclined, beams of light projected down through the centre of the tube, bisecting it and emerging from the downward facing mouth into the water. The two slightly inclined beams were required to compensate for the parallax effect which would otherwise have introduced shadows beside one wall of the tube.

In contrast to the plate experiments it was important here that the tube was placed in the centre of the tank such that the flow in the neighbourhood of the mouth was influenced as little as possible by the presence of the tank walls. However, significant problems were encountered in obtaining a uniform seeding of the water since the particles, once introduced locally, tended to migrate away rapidly and unevenly to the extremities of the tank. In answer to this a thin transparent and extremely pliant plastic bag was used to entirely enclose the working volume of of the experiment and contain the reflecting particles without, it was hoped, interfering with the local fluid behaviour; since no net flows were involved, other than the slow drift associated with progressive waves, this seemed to be a reasonable assumption. Within the enclosure, the seeding was easily maintained at the required concentration by occasional stirring.

Transient tests. In the first series of tests a transient pressure was applied to the fluid in the tube, and the subsequent motions were photographed and measured. The procedure was as follows:

The tube was unclamped from the framework and moved from its equilibrium position, $L = 11$ cm, to a greater depth, for example $L = 15$ cm, where it was re-secured. A sheet of 'stretch-and-seal' plastic film was stretched over the top and drawn down the sides to make an airtight diaphragm. The tube was then lifted up to its equilibrium position and re-clamped to the framework, then containing an elevated column of water with an equivalently reduced air pressure above it, as shown in figure 3. Subsequent removal or puncturing of the stretched diaphragm allowed the air pressure to recover almost instantly to atmospheric, and the fluid

column to fall rapidly, passing its equilibrium point and initiating a series of decaying oscillations. The frequency of free oscillation can be shown to be approximately $\sqrt{(g/L)}$ rad/s, although this is not exact (see Lighthill 1979), and is even further modified here by the nonlinearities associated with the large amplitudes of motion.

Before the visualization tests were begun, a series of tests were performed with the wave probe inserted into the tube. It was incorporated in such a way that the above mentioned test procedure could be enacted; hence a record of the motions was made, while avoiding the aesthetically undesirable appearance of the probe in the visualization photographs. The time responses of these tests were recorded, both directly onto paper, by using a chart recorder, and onto magnetic disk for subsequent retrieval and processing by a computer.

Wave response tests. The behaviour of the fluid column in regular waves was observed by simply holding the tubes at the chosen depth and subjecting them to the required wave conditions. In the cases to be illustrated the wave frequency was chosen to be close to the natural frequency of the tube, thereby exciting the largest amplitude of response.

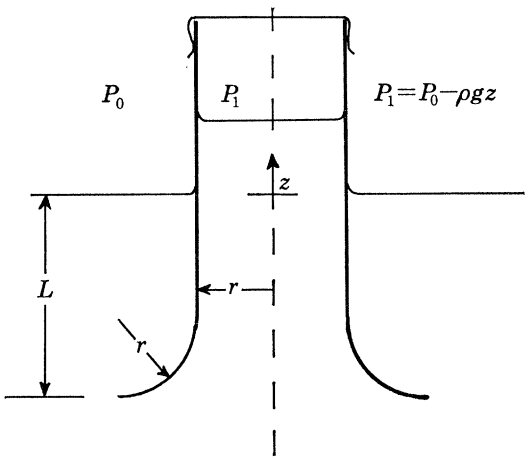

FIGURE 3. Diagram showing essential geometry of 'transient response' experiments.

3.1. EXPERIMENTAL OBSERVATIONS WITH PERIODIC WAVES AND PLATES

Submerged plates

Figure 4 (plate 1) shows a photographic sequence of eddy motions resulting from the passage of regular waves from left to right above a submerged plate. The frequency of the wave was 0.83 Hz, with a crest-to-trough amplitude of 1.1 cm. The surface of the wave can be clearly seen. An exposure time for the photograph of $\frac{1}{8}$ s was chosen to enable sectors of the wave orbital motions to be observed in areas distant from the plate. Schematic diagrams of observed motions near the plate are also shown in figure 5. Starting from the point where the crest of the wave is immediately above the plate, it can be seen from the photograph in figure 4*a* that a small eddy develops immediately behind the trailing edge of the plate. Eddy formation behind sharp-edged plates is well known, and excellent streamline photographs for steady flows have previously been obtained, for example by Prandtl & Tietjens (1934). In terms of water waves the interesting factor results from the progressive rotation of the velocity vector with time (here in a clockwise sense). Figures 4*b* and 5*b* show the situation when the wave has advanced by a quarter of a wavelength. In this part of the motion the eddy is observed to strengthen.

When the trough of the wave is approached, as shown in figures 4*c* and 5*c*. the effect of the orbital motion is clearly seen. At this point the direction of the flow at the edge of the plate has effectively reversed from that when the crest is above the plate. A flow develops between the existing eddy and the plate moving the eddy away from intimate contact with the solid boundary. When the flow becomes sufficiently well developed in the reverse direction a second eddy is initiated on the leading edge of the plate, as shown in figures 4*d* and 5*d*. At this point an eddy (or vortex) pair has been formed.

The final sequence of the motion involves the further rotation of the velocity vector to cause the eddy pair to be thrown off from the plate and projected upwards towards the surface of the

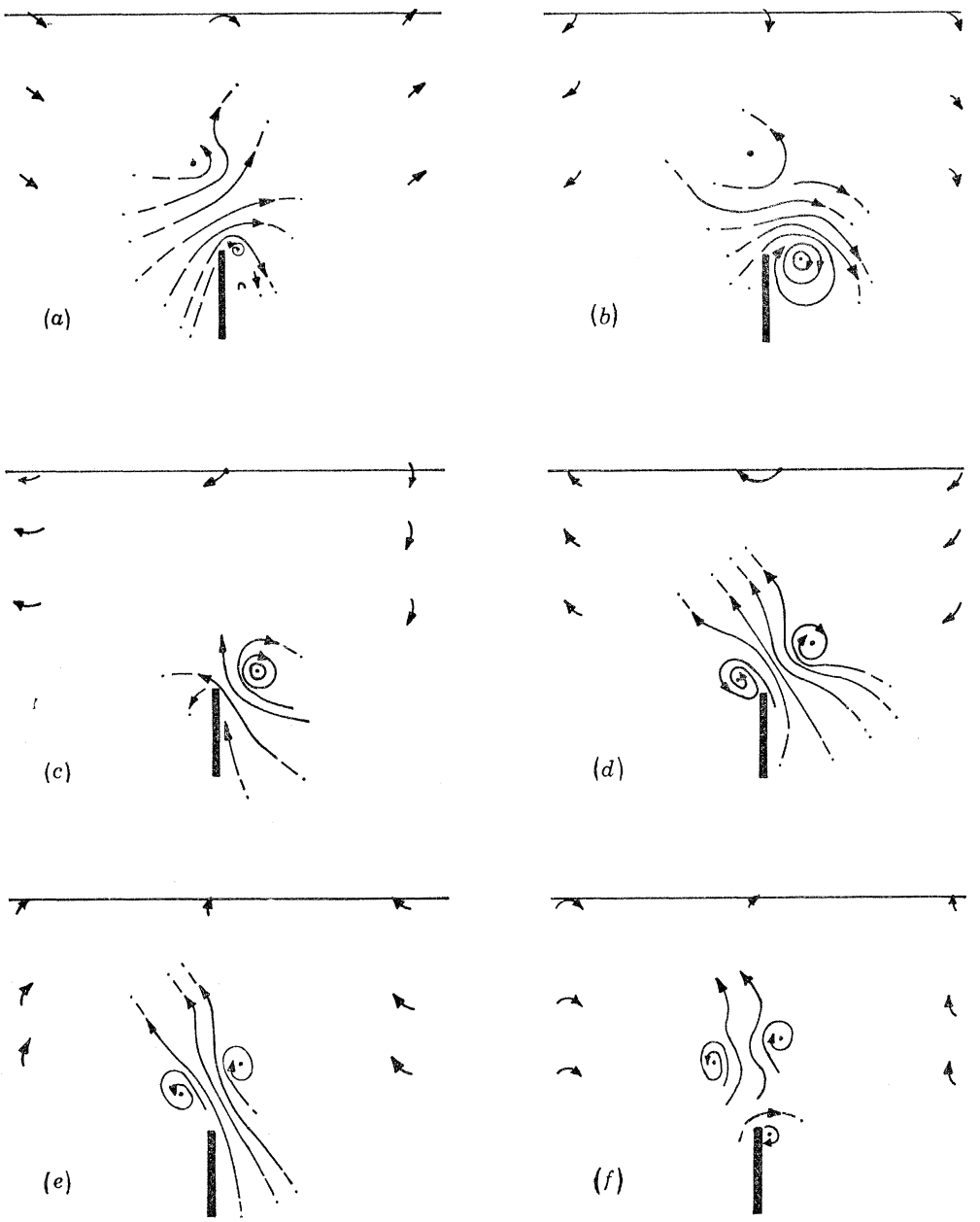

FIGURE 5. Schematic diagram showing the generation of jet eddy pairs associated with wave motion interacting with a submerged plate.

PHILOSOPHICAL TRANSACTIONS OF THE ROYAL SOCIETY A MATHEMATICAL, PHYSICAL & ENGINEERING SCIENCES

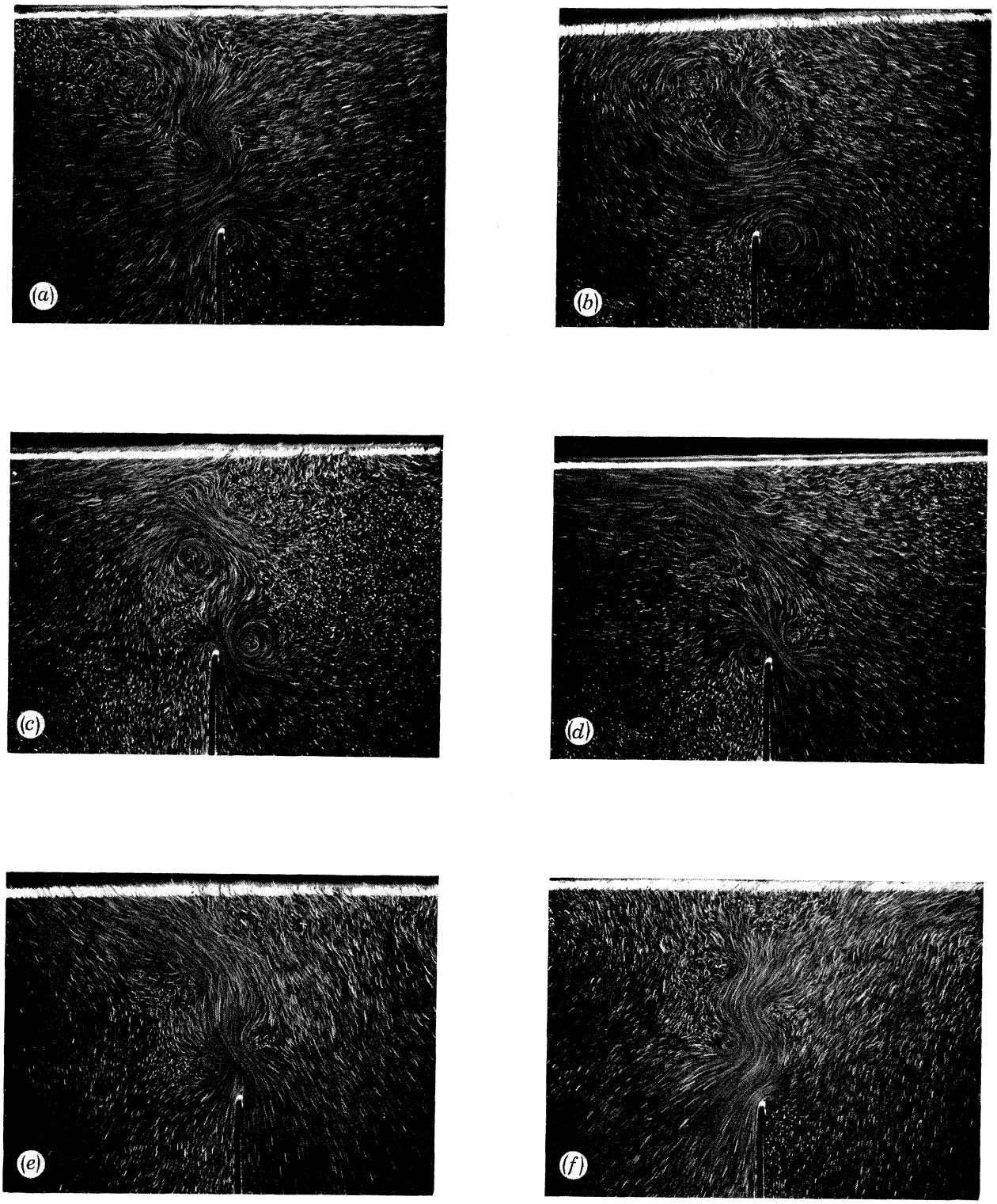

FIGURE 4. Photographs of wave motion interacting with submerged plates. Sequence (*a*)–(*f*) showing development of jet eddy pairs. Wave frequency = 0.83 Hz, wave amplitude = 11 mm. Top of plate 11 cm below surface.

(*Facing p.* 606)

PHILOSOPHICAL TRANSACTIONS OF THE ROYAL SOCIETY A MATHEMATICAL, PHYSICAL & ENGINEERING SCIENCES

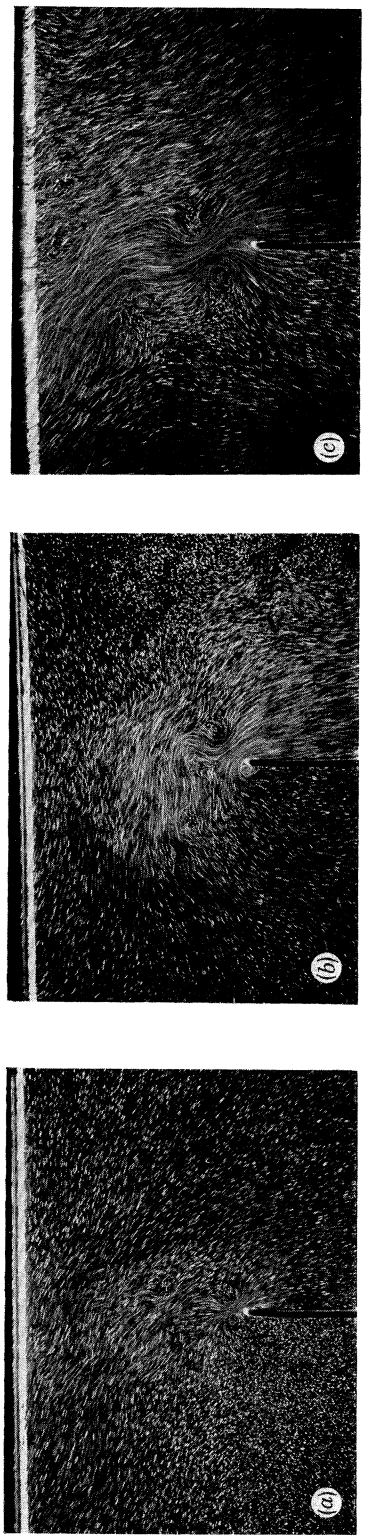

FIGURE 6. Photographic sequence showing the effect of wave amplitude on the intensity of jet eddy pair formation. Wave frequency = 0.83 Hz. Wave amplitude (*a*) = 2 mm, (*b*) = 5 mm, and (*c*) = 11 mm. Other details as figure 4.

FIGURE 7. Photographic sequence of wave motion interacting with surface piercing plates. Bottom of plate 11 cm below surface. Wave amplitude = 11 mm, wave frequency = 0.83 Hz.

PHILOSOPHICAL TRANSACTIONS OF THE ROYAL SOCIETY A MATHEMATICAL, PHYSICAL & ENGINEERING SCIENCES

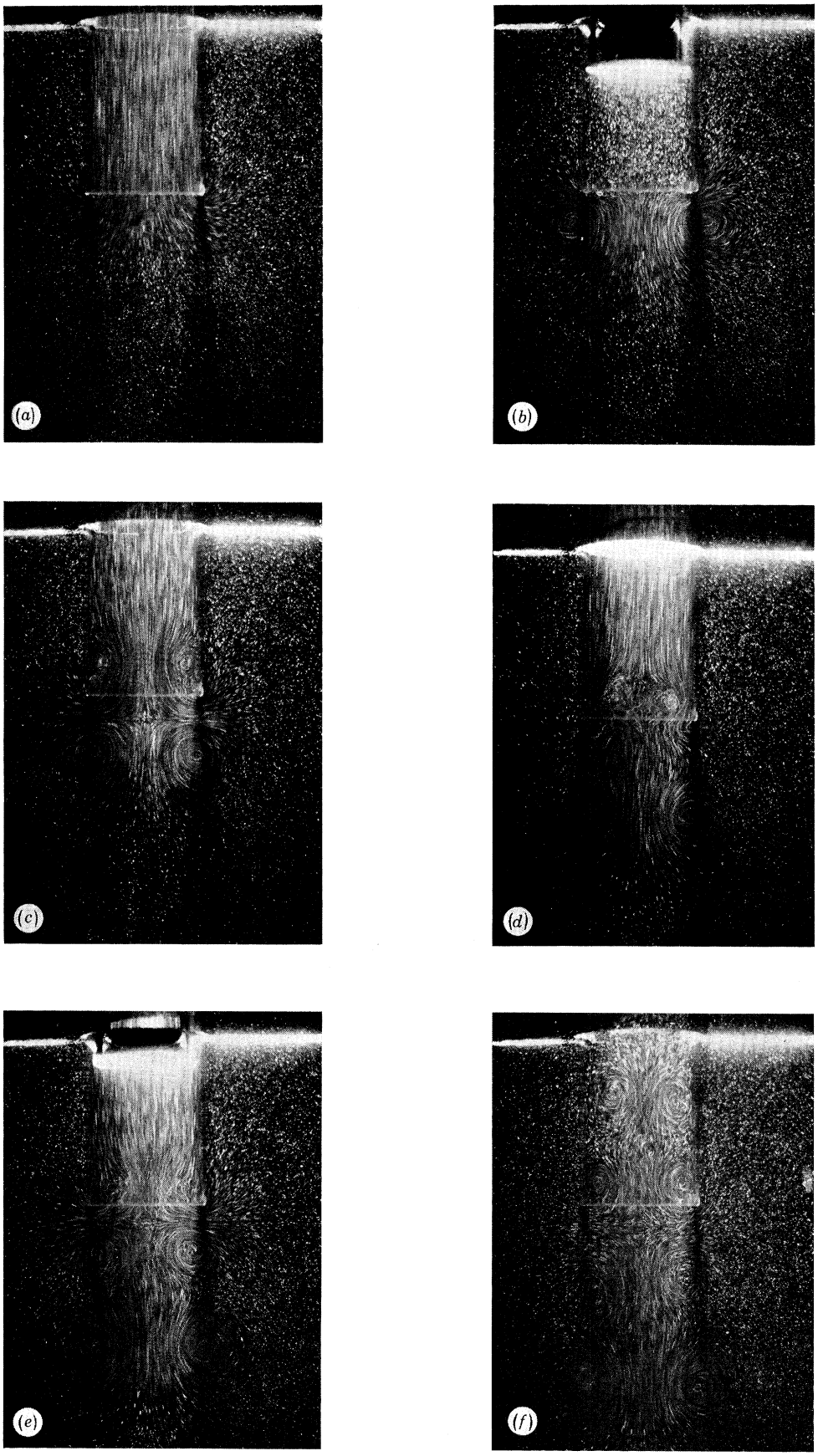

FIGURE 8. Photographic sequence of flow associated with transient response experiment for a parallel-sided tube. Bottom of tube 11 cm below surface. Starting amplitude = 4 cm. Position of each photograph shown in figure 10 *b*.

PHILOSOPHICAL TRANSACTIONS OF THE ROYAL SOCIETY A MATHEMATICAL, PHYSICAL & ENGINEERING SCIENCES

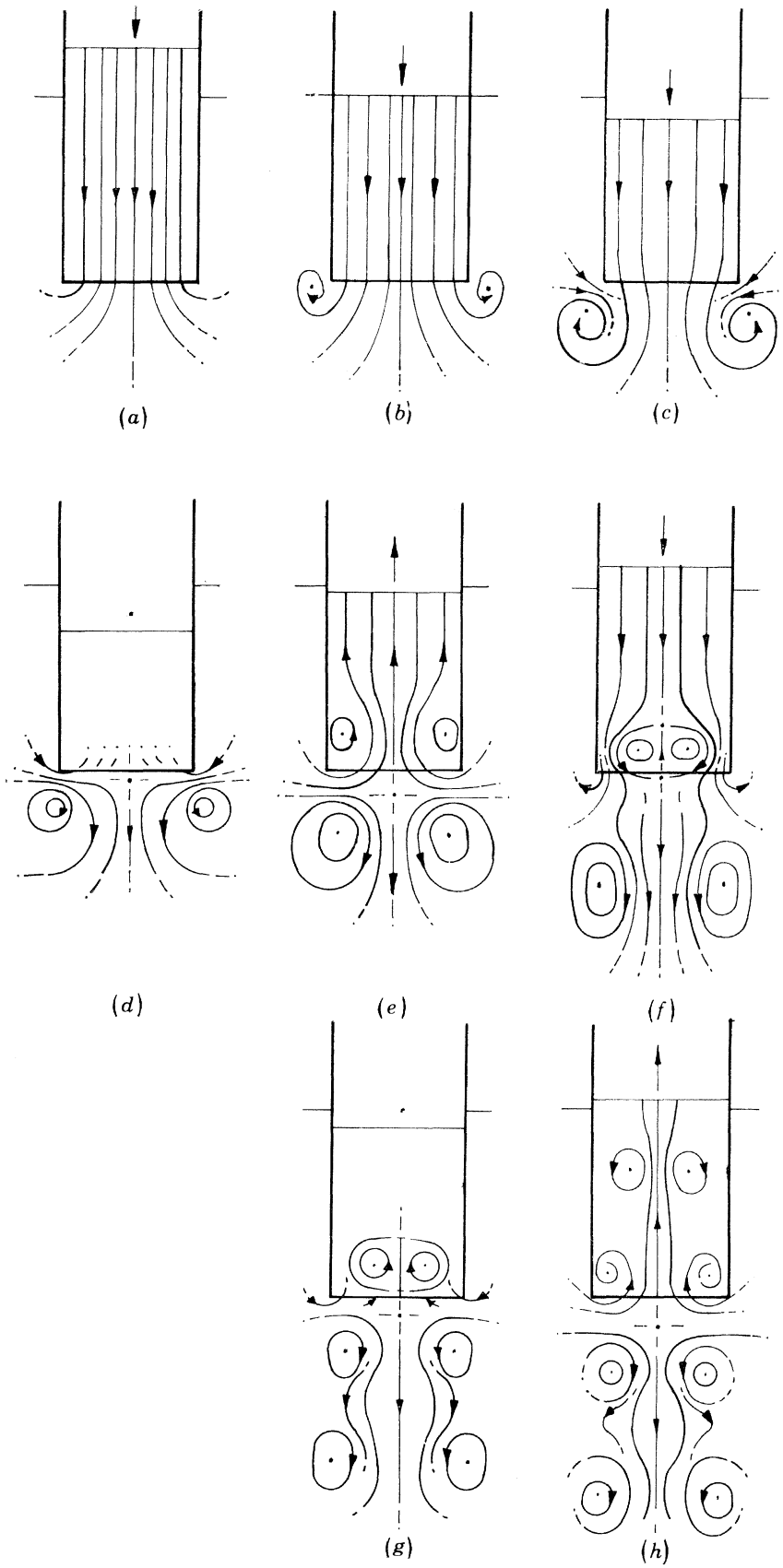

FIGURE 9. Schematic diagram showing the sequence of eddy formation associated with the transient response experiments for a parallel-sided tube.

PHILOSOPHICAL TRANSACTIONS OF THE ROYAL SOCIETY A MATHEMATICAL, PHYSICAL & ENGINEERING SCIENCES

water. We observe the sequence to occur in an essentially similar way for each wave period, consequently one 'jet eddy pair' is formed and ejected into the flow on each cycle.

Velocity measurements of the flow can be estimated either by using the length of individual tracks or, on some photographs, by noting the effect of mains modulation from the Hg lamp; time intervals of 0.01 s will occur between flashes. From photographs such as figure 4*b* it can be seen that velocities at the edge of the plate can be up to four times the orbital velocity of the waves.

The onset of the observed eddy motion depends on dimensional factors which are discussed in § 5. In terms of the dynamic mechanism of eddy shedding, factors such as the wave amplitude and the period, together with the depth of the plate edge below the surface, will become important. The effect of wave amplitude is shown by a sequence of three photographs in figure 6 (plate 2). Each photograph is taken when the wave is at roughly the same position with respect to the plate; as expected, the intensity of the jet eddy pair is increased with amplitude of the wave. The basic mode of ejection of jet eddy pairs appeared similar for all amplitudes. Experiments conducted at different wave frequencies showed slight changes in eddy formation and dissipation. These differences mainly concerned the relative magnitudes of the two eddies; also at higher wave amplitudes than shown in figure 4, after ejection, the eddies sometimes gave the appearance of forming vortex streets similar to the Von Karman vortex street, but convecting in a direction normal to the direction of wave propagation.

Surface-piercing plates

Eddy motions associated with the interaction of regular waves with surface-piercing plates are shown in figure 7 (plate 2). Jet eddy pairs are again observed to form on each wave cycle in a manner similar to that described in the previous section for submerged plates.

Figure 7 shows clearly that in this situation the jet eddy pairs are ejected in a downward direction, and it was noted that tracer particles originally near the water surface and at the side of the plate were quickly 'pumped' by the action of the jet eddy pairs into a region immediately below the plate, leading to an appreciable rectified flow away from the surface. This differed from the case of the fully submerged plate where, conversely, tracer particles originally in the depths were seen to be drawn upwards beside the plate and propelled towards the surface by the rectifying action.

3.2. Experimental observations with surface-piercing tubes

Transient response of parallel-sided tubes

Transient response experiments were conducted at three starting amplitudes with 2, 4 and 6 cm heights of water in the tube. Immediately after flow was initiated by removing the plastic foil from the top of the tube, a sequence of photographs was taken. In order to ensure consistency in the photographs, the experiment was repeated at least twelve times for each of the three starting amplitudes, with each individual experiment consisting of twelve sequential photographs. In all cases the observed flow was quite characteristic and reproducible. A representative series of photographs of one sequence is shown in figure 8 (plate 3): here the starting amplitude is 4 cm, the photograph exposure $\frac{1}{15}$ s and time between each frame 0.27 s. An additional series of schematic diagrams showing the evolution of eddies is shown in figure 9. This diagram was constructed by using information from both the 35 mm and the 16 mm cine photography. Finally, the time response of the surface amplitude in the tube is reproduced in figure 10 for the three amplitudes

PHILOSOPHICAL TRANSACTIONS OF THE ROYAL SOCIETY A MATHEMATICAL, PHYSICAL & ENGINEERING SCIENCES

tested. The approximate positions of the liquid surface in the tube for each photograph shown in figure 8 are indicated in figure 10*b*. (Figure 9 follows its own time evolution). The detailed evolution of eddies shown in figure 8 and 9 can be followed without ambiguity for up to three full oscillations.

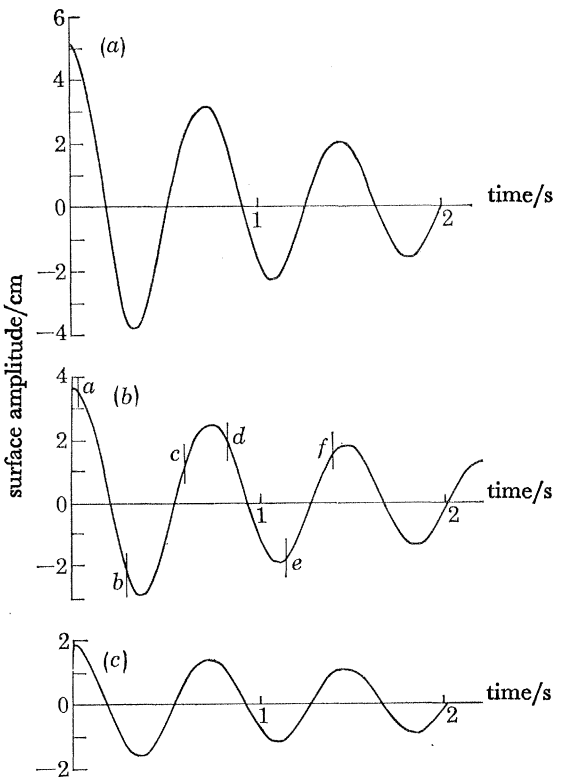

FIGURE 10. Experimental recording of time decay of surface oscillations for the transient response experiments using a parallel-sided tube. Starting amplitudes (*a*) 5.1 cm, (*b*) 3.8 cm and (*c*) 1.9 cm. Letters *a–f* in figure 10*b* indicate approximate positions of surface associated with photographs in figure 8*a–f*.

From rest, the initial downwards motion in the tube as shown in figure 8*a* causes the fluid in the tube to move essentially as plug flow. In § 5 we estimate the thickness of the viscous boundary layer adjacent to the wall to be characteristically less than 1 mm. Our primary concern is with the flow out of, and into, the tube. In figure 8*a* the streamlines of the flow are smooth, radiating outwards from the throat of the tube with a progressive decrease in the velocity. The birth of a small eddy occurs near the outside edge of the tube; with time this eddy strengthens and begins to 'feed' the main flow by drawing fluid between the eddy and the boudary wall into the main stream. The sequence is shown schematically in figures 9*a*, *b* and *c* respectively. Up to this point the evolution of eddies bears a very close resemblance to the generation of fluid (or smoke) rings from tubes as shown in Okabe & Inoue (1960). In contrast to normal smoke ring formation, when the height of the fluid level within the tube is lower than that outside the tube, the fluid in the tube starts to decelerate, stop and reverse. The important point to note is that when the flow reverses, the tube is fed by fluid re-entering from the sides, leaving behind a free vortex ring situated below the tube. As the flow reverses, a characteristic stagnation point, classified by Berry & Mackley (1977) as a hyperbolic critical point, develops at the throat of the flow and is clearly seen in figure 8*c*.

PHILOSOPHICAL TRANSACTIONS OF THE ROYAL SOCIETY A MATHEMATICAL, PHYSICAL & ENGINEERING SCIENCES

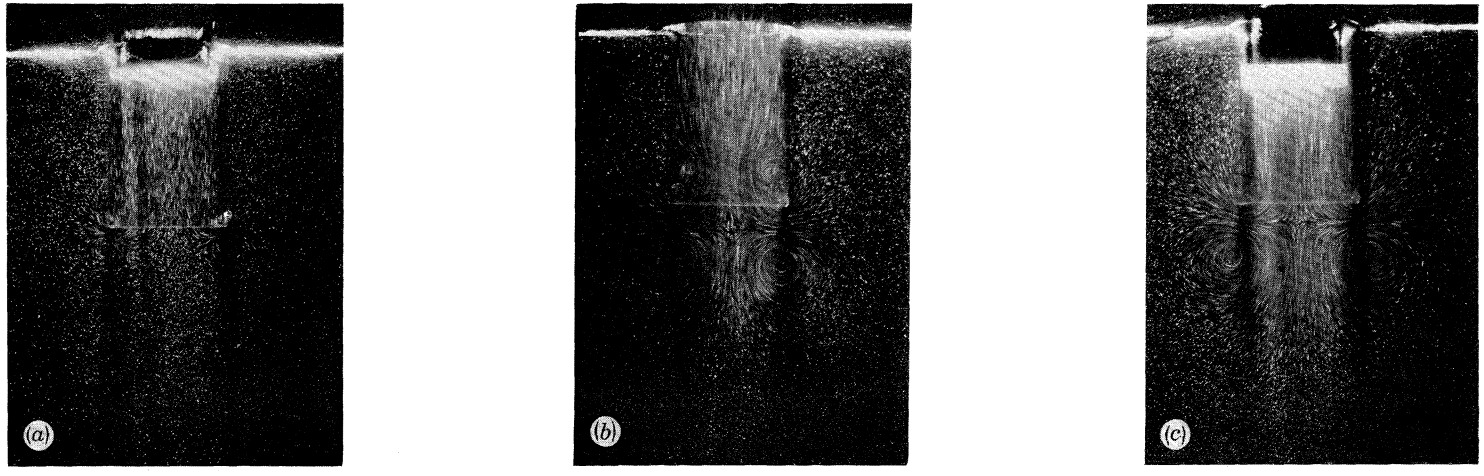

FIGURE 11. Photographic sequence showing the effect of starting amplitude on transient response experiments for parallel-sided tube. Starting amplitude (*a*) = 2 cm, ()*b* = 4 cm and (*c*) = 6 cm. All photographs taken at approximately bottom of first downward stroke. Other details as figure 8.

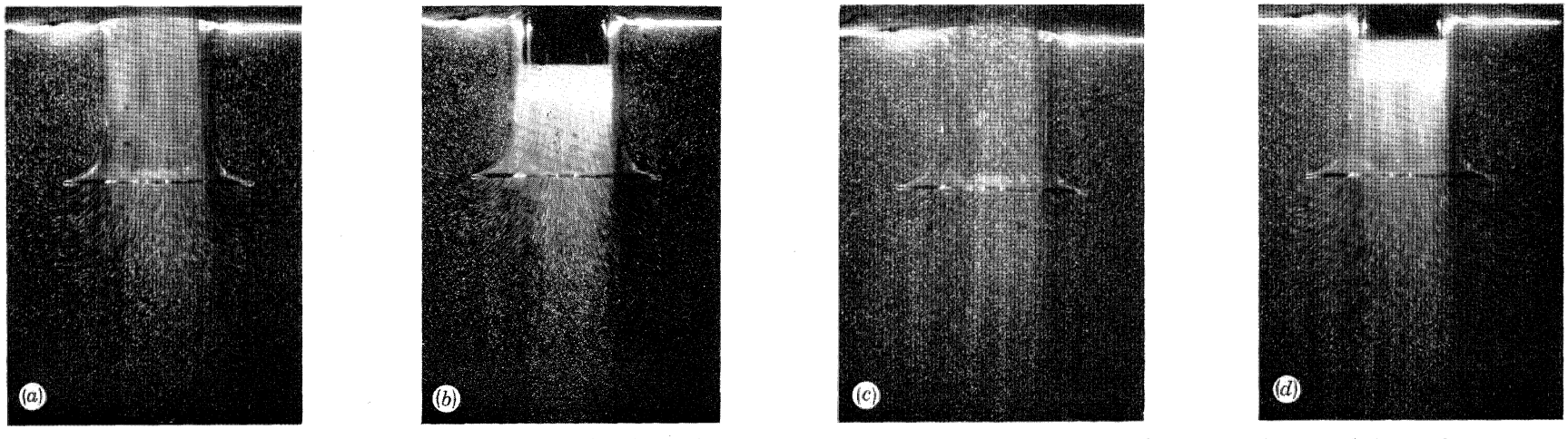

FIGURE 12. Photographic sequence of flows associated with transient response experiment for a bell-mouth tube: bottom of tube 11 cm below surface, Starting amplitude 6 cm, exposure times $\frac{1}{15}$ s. Approximate positions of each photograph shown in figure 13.

FIGURE 14. Photographic sequence of flows associated with tubes interacting with harmonic waves at different points of wave cycle: wave amplitude = 7 mm, wave frequency = 1.4 Hz, bottom of tubes 11 cm below surface, exposure time = $\frac{1}{8}$ s. Figures 14*a–c*, parallel-sided tube; figures 14*d–f*, bell-mouth tube.

PHILOSOPHICAL TRANSACTIONS OF THE ROYAL SOCIETY A MATHEMATICAL, PHYSICAL & ENGINEERING SCIENCES

As the flow strengthens on its upwards movement, the flow separates again and a second vortex ring develops inside the tube. The ring forms initially near the inner walls of the tube. However, when the flow again reverses and starts its second downward movement the vortex ring becomes concentrated into the centre of the flow, and fluid, rather than passing through the ring, is forced between the ring and the inner wall of the tube as shown in figure 8*d*.

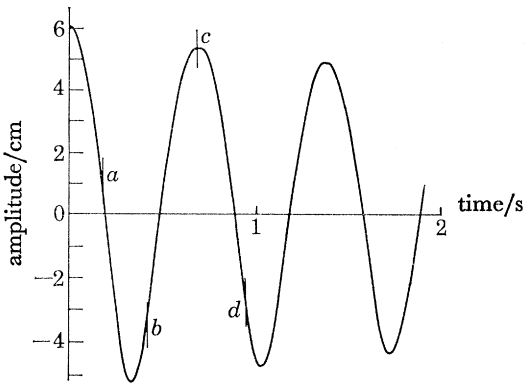

FIGURE 13. Experimental recording of time decay of surface oscillations for transient response experiment using bell-mouth tube. Starting amplitude = 6 cm. Letters *a–c* in figure indicate approximate positions of surface positions of surface associated with photographs in figure 12*a–c*.

On the second downstroke the first vortex ring is forced away from the mouth of the tube and starts its journey to the bottom of the test tank. The second vortex ring remains in the throat of the flow and a third vortex ring forms in a similar way to the first outside the tube (figure 9*g*).

On the second upward stroke the second vortex ring to form is ejected into the body of the flow in the tube and a fourth ring begins to form in a similar manner to the second. All four vortex rings can be clearly seen in figure 8*f*. The evolution of subsequent rings appears to continue with further oscillations. However, because of the rapidly diminishing amplitude of the motion, together with the increasing complexity, positive interpretation becomes difficult.

Finally, the effect of the initial elevation on the transient response is shown in figure 11 (plate 4) where a representative photograph of the flow at the bottom of the first stroke is shown for the three amplitudes tested. It can be seen that only the intensity of the motion, rather than the geometry of the flow, is altered. The energy that the observed eddies extract from the flow is discussed in § 4.

Transient response of bell-mouth tube

The transient response of the bell-mouth tube differed from the parallel tube response both in terms of eddy formation and the decay of the oscillating flow. Figure 12 (plate 4) shows the photographic sequence for the bell-mouth starting from a 6 cm amplitude of elevation. Figure 13 shows the associated motion of the surface with the approximate times of the photographs marked on the trace. The two striking features are the absence of appreciable eddy motions and the considerable reduction in the rate of decay when compared with the parallel tube experiment. From the photographs it can be seen that when the fluid column is at the top of the first upward stroke the flow both inside and outside the tube is essentially at rest. This contrasts with the parallel tube experiment where at the bottom or top of the stroke, the flow in the tube was complex and there were still considerable motions present outside the tube.

The 6 cm amplitude transient was chosen for figure 12 to illustrate a slight indication of eddy-formation at the outer edge on the second downward stroke. However, smaller amplitudes showed no eddy formation and the general motions appeared essentially similar. It can be seen that the flow appears to decelerate uniformly and the region of the flow outside the bell-mouth effected by the motions inside the tube is quite small.

Wave response of parallel sided tube and bell-mouth tube

In figure 14 (plate 5) we show the response of both a parallel sided tube and bell-mouth tube to regular waves of frequency 1.4 Hz and amplitude 0.7 cm. The periodic wave motion induces oscillations of the fluid column within the tube. Figures 14*a*, *b* and *c* show clearly that for the parallel sided tube the flow extending below the mouth consists of a strong irregular eddy motion. The flow within the tube appears fairly regular and strong eddy motions can be seen at the entrance of the tube near the walls. On the upward stroke the eddies appear in the region of the inner wall and on the downward stroke in the region of the outer wall of the tube. The wave motion, which is from left to right in the photographs, appeared to induce asymmetry in that the eddy motion at the leading edge was always observed to be much stronger than that at the trailing edge.

By comparison, figures 14*d* and *e* show the wave response of the bell-mouth tube under identical conditions. No irregular eddy motions are apparent with the flow remaining at all times highly ordered. At the highest amplitude Figure 14*f* does reveal a very small eddy formation near the outside edge of the tube when the flow is directed outwards. Figure 14*e* is particularly interesting showing that, for the bell-mouth tube, when the flow in the tube is effectively stationary, the wave motion outside the tube is essentially unaltered, showing no turbulence; this is certainly not the case for the parallel tube.

4. Energy losses due to eddy motions; a comparison of theory with experiment

In this section we investigate the subject of energy losses through eddy formation and, by relating theory to experimental observations, are able to draw some conclusions as to the practical importance of this form of dissipative action.

Considering first the case of wave interaction with thin vertical plates, the energy balance in these systems can be continuously gauged from the relative magnitudes of the incident, reflected and transmitted waves. By measuring wave elevations at two stations on each side of the duct and taking appropriate steps to compensate for the effects of extraneous wave reflexions from the absorbing beach, a quite accurate picture of the wave field can be derived. This experimental procedure has been described in detail for similar experiments on a fully submerged parallel-plate duct (Knott & Flower 1979). The results of such an analysis show that in both of the cases considered a small but measurable loss of wave energy accompanies the introduction of the plates.

We examine in detail the case of the surface-piercing plate since it is the better suited of the two for analysis. In particular we are able to cover a varied range of test conditions which extend from the reflexion-dominated to transmission-dominated portion of the plate characteristic.

The reflexion and transmission coefficients expressed as the ratios of reflected and transmitted amplitudes to the incident wave amplitude, were measured over a range of frequencies and

amplitudes with the plate fixed at one depth of immersion. The results are plotted in figure 15 as a function of the period parameter $\omega^2 a/g$, where ω is the angular frequency, a is the depth of the plate edge below the surface and g is the gravitational constant. The amplitude of the incident wave was normally about 3 mm trough-to-crest. At one value of the period parameter, 0.64, the test was repeated at four amplitudes ranging from 2 to 8 mm; the resulting coefficients showed some scatter, as indicated in the figure, but no consistent trend with amplitude. Also plotted in in figure 15 are corresponding coefficients derived from linear theory by Ursell (1947). A measure of the net energy dissipation in the system can be assessed from a term defined as the ratio of the total energy in the departing waves to the energy in the incident wave. This is simply expressed as the sum of the squares of the reflexion and transmission coefficients, and is illustrated in figure 16.

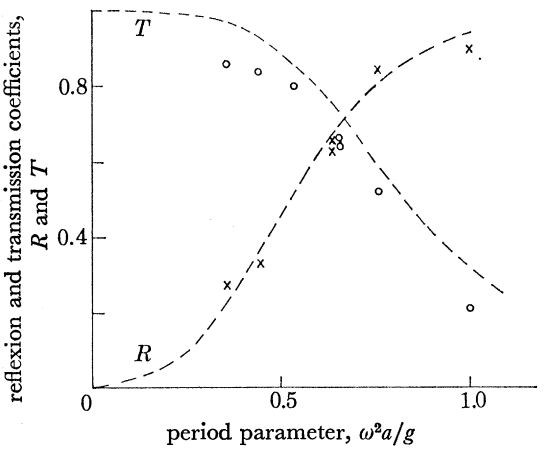

FIGURE 15

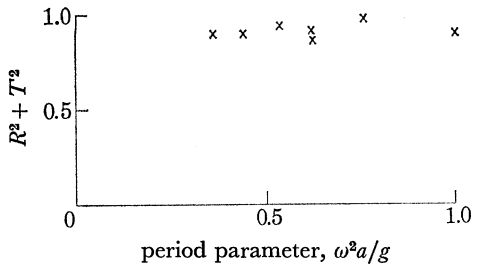

FIGURE 16

FIGURE 15. Reflexion (R) and transmission (T) coefficients for the surface piercing plate as a function of period parameter. At one value of the period parameter, 0.64, the experiment was repeated at four wave amplitudes. The resulting variation in the coefficients is indicated by the connected symbols. The continuous lines represent linear theory (Ursell 1947).

FIGURE 16. The energy coefficient $R^2 + T^2$ as a function of period parameter.

With the exception of one point which occurs at a frequency close to the cross-wave resonance of the tank, the energy coefficient indicates a deficit of between 5 and 12 %. Some portion of this loss occurs naturally as a result of fluid friction serving to attenuate the wave between the measurement points. This loss, which is frequency dependent, may be large enough to dominate over eddy losses at the plate. However, while a figure could be quoted here from prior measurement it would be misleading in the context of the present experiment to do so since the degree of uncertainty involved is, when squared, comparable to the magnitude of the effect under observation. Hence we do not attempt to differentiate between the two sources of loss. In view of this, these experiments are of limited use for the estimation of eddy energy, but we can at least state that an upper limit appears to exist, and that this bound of about 10 % appears to be insensitive to the wave amplitude and frequency.

Greater certainty surrounds the relative magnitudes of transmission and reflexion since they should be reduced in equal proportion by propagation attenuation. The question had previously been asked as to whether the energy taken up by the eddies was given at the expense of the

transmitted or the reflected waves. The results shown here strongly suggest the former. They are quite consistent in showing the transmission coefficient to fall well below the theoretical value, while the reflexion coefficient equals and sometimes exceeds it. Indeed this latter fact tends to indicate that the reflexions are, if anything, increased as a result of the eddy shedding, since the coefficient is as it stands an underestimate of the true value of the extent of the propagation loss.

In practical terms the loss of energy in transmission may be viewed as a loss in the mean flux of fluid kinetic energy crossing the sharp edge; the fact that there is little change in the coefficient over a range of wave amplitudes at fixed frequency suggests that the flux of kinetic energy is dissipated in fixed proportion, independent of amplitude, as might have been expected. The dependence on depth, and hence frequency, is at present obscured by the uncertainties outlined above.

A direct estimation of the energy bound up in the vortices by inspection of the photographic evidence would have been particularly helpful, but without a realistic estimate of the radius of the eddy cores (imperceptible here) this could not be accurately accomplished.

In concluding this investigation of losses at plates it is clear that only a small proportion of wave energy is dissipated in eddies at a single plate. Hence eddy formation is unlikely to seriously reduce the efficiency of plate-like wave energy converters. It will, however, increase fluid loading, not only the fluctuating wave forces but also the mean forces that can be expected. Mean forces may be estimated from the momentum balance of incident, reflected and transmitted waves, as described by Longuet-Higgins (1977). Clearly an increase in reflexion and a decrease in transmission will serve to increase the mean force on the plate, and we would expect it to exceed the theoretical value by a significant amount. These comments are not ideally supported by the results presented by Cooper & Longuet-Higgins (1951) for a similar series of experiments in which significantly reduced reflexion coefficients were measured. However, the disparity is thought to be largely a matter of scale. Their results indicated reflexion coefficients to be between 0.72 and 0.95 of the theoretical values, attributing the loss to dissipation at the sharp edge of the plate. However, in contrast to our experimental method, their procedure was to vary the depth of immersion of the plate (between 2 and 10 cm) while keeping the wavelength constant ($\lambda \approx 30$ cm). This, in effect produced a relative reduction in the scale of their experiments at the lower values of the frequency parameter $\omega^2 a/g$ where the most notable discrepancies occurred.

We now turn to eddy losses in the ducted flow experiments. These are more amenable to accurate analysis since the formation of eddies has a stronger influence on the overall fluid motions, and the rate of energy extraction from the system is more accurately observable. The significance of the energy losses due to eddies is clearly shown in figure 17, which illustrates the transient responses of the bell-mouth and sharp edged tubes operating in similar conditions. The attenuation of the oscillations in the latter case is quite marked.

We employ throughout time domain methods, (in which solutions are expressed as a function of time), using the transient response as the basis for investigation. A similar series of experiments has previously been investigated by Lighthill (1979) who used linearized frequency domain methods to estimate the magnitude of flow losses. In that case measurements of steady-state oscillations in surface-piercing tubes in response to regular waves formed the basis for analysis, and non linearities were investigated by varying physical parameters and using extrapolation techniques. This necessarily required certain approximation, but led to an economical and direct interpretation of the data.

PHILOSOPHICAL TRANSACTIONS OF THE ROYAL SOCIETY A MATHEMATICAL, PHYSICAL & ENGINEERING SCIENCES

Here we have chosen to use time domain methods, despite their added complexity, since they allow the system to be closely observed at successive instances, and allow the inclusion of non-linear terms in the equations of motion. The solution of these equations is accomplished by using a digital computer. The hydrodynamic model simplified to its essentials is shown in figure 18.

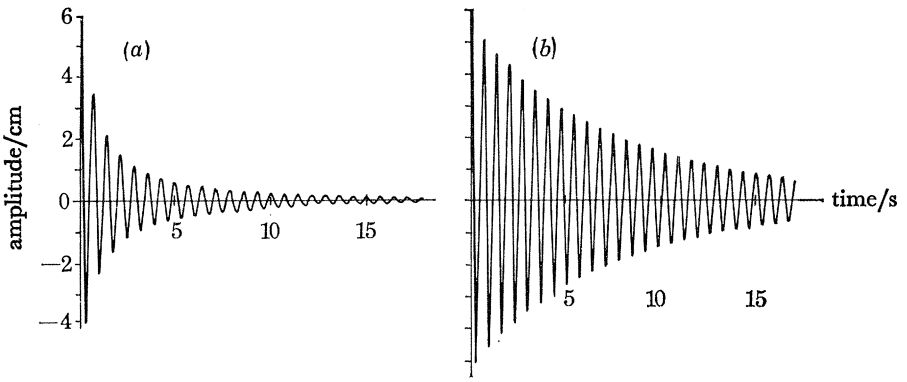

FIGURE 17. Comparison of the experimentally observed time decay of oscillations for the transient response experiment. Starting amplitude in both cases is 6 cm. Figure 17*a*, parallel-sided tube; figure 17*b*, bell-mouth tube.

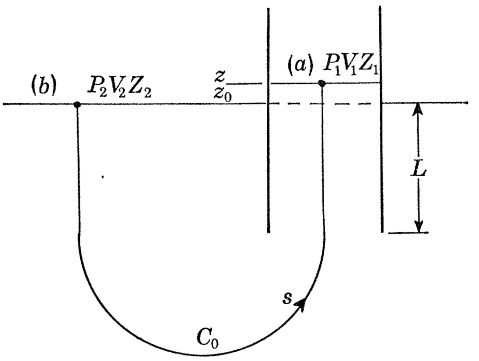

FIGURE 18. Schematic diagram of computer simulation model for transient response experiments.

We consider the case of a tube immersed to a depth L in the free-surface of a semi-infinite ideal fluid. The tube is assumed to be sufficiently narrow to avoid significant wave motion at the internal free-surface. A line C is drawn from the exterior to the interior on which the motion of fluid particles may be described by the unsteady form of the Bernoulli equation

$$\int_c \frac{\partial V}{\partial t} \mathrm{d}s + \tfrac{1}{2}V^2 + \frac{P}{\rho} + gZ = \text{constant}. \tag{4.1}$$

The 'unsteadiness' is accounted for here by the scalar product within the line integral which represents the additional gradient of excess pressure due to local fluid acceleration. We identify the two terminal points as being on the interior free-surface at (*a*), and on the exterior surface at (*b*) which is chosen to be far enough away for the velocity and surface displacement there to be negligibly small. Then,

$$\frac{P_2}{\rho} + gZ_2 = \int_b^a \frac{\partial V}{\partial t} \mathrm{d}s + \tfrac{1}{2}V_1^2 + \frac{P_1}{\rho} + gZ_1. \tag{4.2}$$

Let

$$Z_1 = Z_2 + z,$$

$$P_1 = P_2 + p,$$

where z and p are respectively, perturbations in elevation and pressure within the tube. Equation (4.2) then becomes

$$0 = \int_b^a \frac{\partial V}{\partial t} \mathrm{d}s + \tfrac{1}{2} V_1^2 + \frac{p}{\rho} + gz. \tag{4.3}$$

We need to evaluate the integral in equation (4.3), which represents in mechanical terms the reaction of a 'virtual' mass; that is to say, the mass in the tube plus an end effect.

In general, the equation allows the tube to be of varying cross section, but here a simplifying assumption is made that the tube is uniform and of area A_1. In asserting this it becomes possible to treat the integral in equation (4.3) in two halves; from (b) to the equilibrium position at z_0, wherein the integrand may be arbitrarily defined; and from z_0 to z wherein the integrand is constant. Hence,

$$\int_b^a \frac{\partial V}{\partial t} \mathrm{d}s = \int_b^{z_0} \frac{\partial V}{\partial t} \mathrm{d}s + \int_{z_0}^{z} \frac{\partial V}{\partial t} \mathrm{d}s \tag{4.4}$$

$$= l_1 \, \mathrm{d}V_1/\mathrm{d}t + (z - z_0) \, \mathrm{d}V_1/dt. \tag{4.5}$$

Let,

$$l_1 = L(1+\epsilon),$$

$$z_0 = 0,$$

where l_1 is an 'effective' length of tube and ϵ is an added increment.
Then equation 4.3 becomes

$$0 = \{L(1+\epsilon) + z\} \, \mathrm{d}V_1/\mathrm{d}t + \tfrac{1}{2} V_1^2 + p/\rho + gz. \tag{4.6}$$

A further three terms must now be added to account for damping.

The first arises from the loss of energy through surface wave generation. This 'radiation damping' is directly related to the rate at which waves are generated and radiated by the oscillating flow, and is a complex function of geometry and frequency. Nevertheless, for any physical system the radiation damping can be uniquely determined by the proper application of potential theory, and is not dependent on dissipative action. It is assumed here to act linearly (for small amplitudes) and is included as a pressure term serving to oppose motion in phase with and proportional to velocity. For convenience it is introduced as a component of the excess pressure in the tube p, rather than at the exterior free-surface since the velocity there is undefined:

$$p_{\mathrm{d}1} = C_{\mathrm{r}} V_1. \tag{4.7}$$

Internal fluid friction is the second source of damping and is rather uneasily reconciled with the foregoing ideal fluid equation since it is, unlike radiation damping, the product of a non-ideal fluid. Its action is unevenly distributed through the fluid being localized in the boundary layer at the walls, but its practical effect on pipe flows is to cause a resistance to motion equivalent to a loss of pressure, and it is included here as a 'lost head' term. In fully developed steady flows resistance coefficients have long been established. In oscillatory flows rather less is known, but it is reasonable to assume, as demonstrated in § 5, that the lost head in the case considered here can be represented by a velocity-proportional pressure acting to oppose motion in a similar mode to radiation damping.

$$p_{\mathrm{d}2} = C_{\mathrm{f}} V_1. \tag{4.8}$$

The third term is that due to the dissipative action of eddy shedding. As a first approximation we introduce it as an additional lost head term.

$$p_{\mathrm{d}3} = K(\mathrm{sgn}\, V) \tfrac{1}{2} \rho V_1^2, \tag{4.9}$$

where the constant of proportionality K represents the fraction of the kinetic energy flux across the mouth that is lost in eddies, and the (sgn V) ensures that the pressure acts in the correct sense. In the simulation this term is divided into two and made directionally dependent in order to observe whether the mechanism of eddy damping is sensitive to the direction of flow.

$$p_{d_3} = \begin{cases} \frac{1}{2}K_1\rho V_1^2, & V_1 > 0, \\ \frac{1}{2}K_2\rho V_1^2, & V_1 < 0. \end{cases} \tag{4.10}$$

Since equation (4.1) only applies to irrotational flow the approach adopted here may be deemed to be invalid for cases where eddy motion occurs, and this shortcoming is duly recognized. It is arguable, however, that realistic results may still be obtained if a path is chosen that avoids concentrations of vorticity, and in the case considered here it is of interest to note that a path could exist on or near to the axis of the tube, which, for reasons of symmetry, complies with the condition that the flow is irrotational.

A fourth damping term due to surface tension is not thought to be significant in these experiments, and is omitted.

The full simulation equation is now

$$-\frac{p_f}{\rho} = \{L(1+\epsilon)+z\}\frac{\mathrm{d}V_1}{\mathrm{d}t} + gz + \left(\frac{C_r+C_f}{\rho}\right)V_1 + \tfrac{1}{2}V_1^2 + \begin{cases} \frac{1}{2}K_1(V_1^2), & V > 0, \\ \frac{1}{2}K_2(V_1^2), & V < 0, \end{cases} \tag{4.11}$$

where p_f is a forcing pressure, and z is instantaneously evaluated as

$$z(t) = \int_0^t V_1(\tau)\,\mathrm{d}\tau. \tag{4.12}$$

It is convenient at this point to introduce a simple linearized model which bears comparison with the above equation for small amplitudes of motion and which can, by virtue of its common occurrence in mechanics, act as a useful analogy for the purpose of defining certain parameters.

The equation written below is for a second-order damped mass/spring system in which the 'mass' is the mean mass of water within the tube and the 'spring' is the restoring force due to gravity.

$$-p = \rho L\ddot{z} + C\dot{z} + \rho g z, \tag{4.13}$$

from which the 'natural frequency' of free oscillation is given by

$$\omega_n = \sqrt{(g/L)}, \tag{4.14}$$

and the damping ratio by

$$\xi = C/2\rho\sqrt{(gL)}. \tag{4.15}$$

This latter term expresses in non-dimensional form the relative magnitude of the damping in the system and uniquely determines the 'band width' of the system. It may also be written as

$$\xi = C/C_{\mathrm{crit}}, \tag{4.16}$$

where C_{crit} is the critical damping coefficient at which transient motion is just brought to rest without overshooting the equilibrium position; or alternatively,

$$\xi = \frac{1}{4\pi}\frac{\text{energy extracted per cycle of forced oscillation}}{\text{net energy participating in the cycle}}. \tag{4.17}$$

When dealing with nonlinear damping this latter definition can be employed to produce an 'effective' damping ratio even though the definitions of equations (4.15) and (4.16) are not valid, since the mean energy extraction rate has a physical significance that can generally be calculated from equation 4.17 and that admits a comparison of the practical effects of different damping terms.

PHILOSOPHICAL TRANSACTIONS OF THE ROYAL SOCIETY A MATHEMATICAL, PHYSICAL & ENGINEERING SCIENCES

The computer program. The program was written in SL1 simulation language for operation on a Xerox Σ5 computer. The integration step length was chosen to be 5×10^{-3} simulation second, which determined in practice that 130 integrations were performed for each cycle of free oscillation of the system. At this integration rate the response was computed at approximately one second per simulation second.

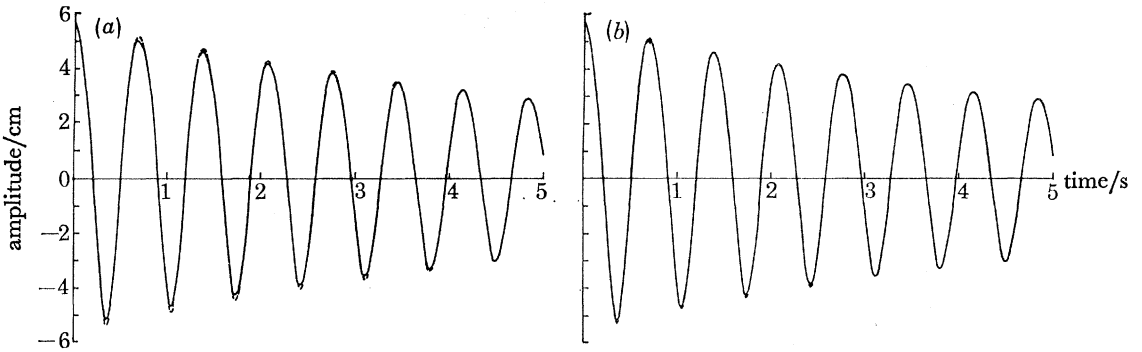

FIGURE 19. Comparison of experimental and simulation response for the time decay of surface oscillations for the transient response experiment using a bell-mouth tube. Starting amplitude = 6 cm; simulation parameters: figure 19*a*: $L = 0.11$, $\epsilon = 0.09$, $\xi = 0.015$, $K_1 = 0$, $K_2 = 0$; figure 19*b*: $L = 0.11$, $\epsilon = 0.09$, $\xi = 0.011$, $K_1 = 0$, $K_2 = 0.12$.

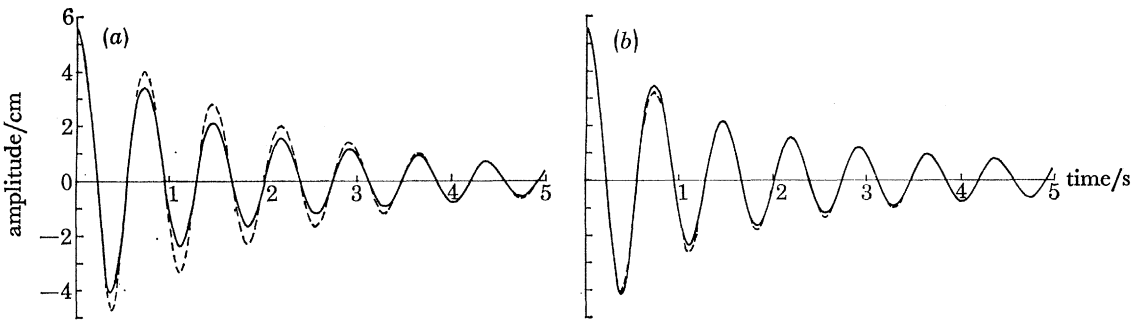

FIGURE 20. Comparison of experimental and simulation response for the time decay of surface oscillations for the transient response experiment using the parallel-sided tube. Starting amplitude = 6 cm; simulation parameters: figure 20*a*: $L = 0.11$, $\epsilon = 0.19$, $\xi = 0.06$, $K_1 = 0$, $K_2 = 0$; figure 20*b*: $L = 0.11$, $\epsilon = 0.19$, $\xi = 0.025$, $K_1 = 0.90$, $K_2 = 0.96$.

In the experiments the system was set in motion by applying a step change in pressure P at the free surface in the tube, having previously elevated the surface by applying an equivalent negative pressure. In the simulation an exactly analogous procedure is adopted to initiate the motion by prescribing appropriate initial conditions. In neither case is any further external stimulus applied to the system after the onset of motion. Having previously recorded the response of the real system in the computer memory, both the real and simulated responses were displayed simultaneously on the computer graphics terminal. Then the latter was modified by changes in the appropriate parameters and re-computed until the best possible agreement was reached between the two results. This required adjustment of the oscillatory period, principally by means of ϵ, and modification of the decay rate by means of ξ, K_1 and K_2.

Results. The experimental and theoretical results from the bell-mouth tube as illustrated in figures 19*a* and 19*b* are superimposed to facilitate comparison between the measured and computed responses. In the first case, figure 19*a* only linear damping is used. While adjustment of this

parameter allows the amplitudes to coincide at the end of the record, agreement in the earlier part of the trace is only moderate. In figure 19*b* the response has been further optimized by introducing some nonlinear damping on the outflow, and agreement overall is excellent.

The response from the straight edged tube is, as expected, considerably less well behaved. Figure 20*a* illustrates how poorly the simulation compares with experiment when only linear damping is introduced. In this case the damping has been adjusted such that the responses coincide at the beginning and end of the record. But even with this artificially large amount of linear damping, the rapid decay of the first few periods cannot be reproduced.

After the introduction of an appropriate degree of nonlinear damping the response in figure 20*b* was achieved. The coefficients on in-flow and out-flow were respectively 0.9 and 0.96, which may be interpreted as meaning that 90 and 96 % respectively of the kinetic energy flux across the mouth of the tube is dissipated in eddies; figures that agree closely with those deduced by Lighthill (1979) on analysing data from surface piercing tubes provided by Vickers Ltd., and that are close to the 'total loss' often quoted for abrupt exits and entries. The ability of the simulation to reproduce the behaviour of the experimental model inspires confidence in these results, particularly in accommodating the nonlinear contribution from the time-varying mass, which leads to the asymmetry in the motion as seen in figures 19*a* and 19*b*. In addition, the solutions arrived at above are arrived at unambiguously since the four controlling parameters act independently.

Finally, we can comment on the energy bound up in the free vortices that are observed to form with the parallel tube experiments. We are in the position of knowing the energy that has gone into the formation of a vortex ring, that is, if we are justified in assuming that the energy lost from the dynamic head is largely incorporated in the eddy; hence we can estimate the size of the core from measurements of the local velocities.

In the case which we have compared with the simulation, the kinetic energy lost on the downstroke is estimated from the integral,

$$K_2 \int_0^T \tfrac{1}{2}\rho A |V| V^2 \,\mathrm{d}t, \tag{4.18}$$

to be 0.021 N-m, where T is the time at the first reversal of flow. The energy bound up in an 'ideal' vortex ring can be determined from the expression given in Batchelor (1970),

$$E = \tfrac{1}{2}\rho\alpha\Gamma^2 \ln \alpha/\sigma, \tag{4.19}$$

where α is the radius of ring, σ the radius of core, and Γ the circulation $= 4\pi \mathrm{d} V$, where d is the distance from centre and V the velocity at d.

We have estimated the velocity distribution of the vortex ring of the form illustrated in figure 11*c* and calculated the mean circulation to be

$$\Gamma = 0.016 \text{ M}^2/\text{s}.$$

Using equation 4.19 and the derived values of E and Γ we arrive at a value of

$$\sigma = 1.1 \text{ mm}.$$

An independent figure can be arrived at if we are to assume that the oscillating boundary layer detached at the mouth becomes wholly incorporated in the core. If the thickness of the boundary layer is of order $D = (\nu/\omega)^{\frac{1}{2}} \approx 0.4$ mm and the core has a cross sectional area $\pi\sigma^2$ of order $2\hat{z}D$, then, with $\hat{z} = 4$ cm, $\sigma \approx 3$ mm. While our photographs contain insufficient detail to confirm the accuracy of either of these estimates, it would appear that a core radius of order 1 mm is in reasonable agreement with expectations.

PHILOSOPHICAL TRANSACTIONS OF THE ROYAL SOCIETY A MATHEMATICAL, PHYSICAL & ENGINEERING SCIENCES

5. The relative magnitude of energy losses and the importance of scale

In this section we make a quantitative comparison of the relative magnitude of energy losses due to radiation, frictional and eddy damping, related in particular to the efficient operation of resonant wave-energy converters, and to the manner in which the losses and the experiment may scale.

The subject of resonant tube converters has received recent attention from Lighthill (1979) who, among others factors, develops an appreciation of damping and external losses. Lighthill shows that in any second order linear system, the optimum extraction of useful energy occurs when the internal damping (due to the energy extraction machinery) is equal to the sum of all the other damping terms and that the energy conversion in the case of the resonant tube in water waves is maximized when the extraneous 'loss' terms are minimized with respect to the radiation damping.

Radiation damping. The non-dimensional radiation damping ratio, ξ_r, is the standard by which we compare the contribution of other damping terms. It is not related to scale since it is purely a function of geometry and can be evaluated by the application of idealized potential flow theory.

Figures for radiation damping coefficients have been evaluated for two dimensional ducts by Lighthill (1979). However, the present case differs not only in being 'three dimensional', but in being influenced by the presence of the tank walls. In the absence of an adequate extension to cover this we cannot present an accurate figure from theory. From the preceding experimental analysis we have derived values for the linear damping ratio ξ (radiation plus linear friction) to lie between 0.011 and 0.025 for the two duct geometries tested. While we cannot separate the contribution from friction in these experiments we show in a later section that theory predicts the friction damping coefficient ξ_f, to be of the order 0.005. We thus feel justified in quoting a value of 0.015 as being representative of the order of magnitude of the radiation damping for the two experiments.

Eddy damping. Since the mechanism is nonlinear, it is inappropriate to derive a value or even an average value for the eddy damping ratio ξ_e from equation (4.15). Instead, we may use the definition given in equation (4.17) to derive a representative figure for the ratio from a consideration of the net magnitude of energy lost in a cycle relative to the mean value of stored energy. Here we consider the fluid column to be forced to oscillate with a constant frequency ω, and amplitude $\hat{z}$ in simple harmonic motion.

The net energy lost in eddies per cycle is derived from the integral of that proportion of the kinetic energy flux across the mouth which is assumed to be dissipated, hence

$$E_e = \int_{\text{cycle}} \tfrac{1}{2} K A \rho |V^3| \, dt. \tag{5.1}$$

Using appropriate values of K taken from the 'transient response' simulation for the parallel-sided tube,

$$K = 0.90, \quad V > 0,$$

$$K = 0.96, \quad V < 0,$$

and defining

$V = \hat{z}\omega \cos \omega t$, $A = \pi r^2$, where r is the radius of tube, we arrive at

$$E_e = 1.24 \rho \hat{z}^3 \omega^2 \pi r^2, \tag{5.2}$$

The net energy in the system can be written in terms of the kinetic energy only when the potential energy is zero, thus

$$E_n = \tfrac{1}{2}\pi r^2 L\,\rho(\hat{z}\omega)^2. \tag{5.3}$$

Using equations (4.17), (5.2) and (5.3), the eddy damping ratio is given by

$$\xi_e = 0.2\,\hat{z}/L. \tag{5.4}$$

If we introduce the dimensionless number $K_z = \hat{z}/L$, which represents the ratio of oscillation amplitude to tube length,

$$\xi_e = 0.2\,K_z. \tag{5.5}$$

In our experiments, if oscillations of ± 4 cm were to be sustained in the tube of length 11 cm, $K_z = 0.36$, and hence $\xi_e = 0.071$, which, when compared with the radiation damping ratio $\xi_r = 0.015$, well illustrates the dominating influence of this term at high amplitudes. At low amplitudes, $K_z < 0.01$, it diminishes to insignificance, ultimately vanishing. When the preceding analysis is repeated for the case of the bell-mouth oscillating at ± 4 cm, we arrive at a figure of $\xi_e = 0.0046$ for the eddy damping ratio, which is now significantly smaller than the radiation damping ratio, confirming in numerical terms the great improvement effected by the change of geometry.

In formulating appropriate similarity laws for eddy losses it would be convenient to be able to assume that the fluid mechanisms and the proportion of lost pressure-head are substantially independent of scale, since this would eliminate any further considerations ensuring the exclusiveness of the z/L parameter. This might be realistic when dealing with the simple case of a sharp-edged duct, since at a sharp-edge the mechanism of separation and eddy formation is hardly affected by scale; but in practice, the presence of finite curvatures will necessarily modify the flow, leading at a sufficiently large curvature to the eventual elimination of separation as is witnessed in the case of the bell-mouth, so it is necessary to establish an additional scale dependence in these intermediate cases when the separation of flow is contingent upon dimensional factors.

First, the constitution of the boundary layer, whether it is laminar or turbulent, plays an important part in determining the conditions for separation. In steady flows similarity in terms of Reynolds number can often be arranged, either by adjusting physical variables or by artificially inducing turbulence, and a similar if more complex approach could doubtless be employed in the unsteady case. But while adherence to similarity in this respect is advisable it is arguable whether it is absolutely necessary in the present case, since small scale models will, if anything, give conservative figures for losses compared with oceanic devices where a transition to turbulence is likely to delay separation and reduce eddy motion.

The second question, which we now investigate, is whether the time-dependent nature of the flow itself imposes significant additional demands on experimental similarity. We are able to gain an initial insight into the mechanics of unsteady separation by considering a mathematical description of the flow. We do not examine the particular case of the bell-mouth geometry since this is both too complex and too specialized. We consider instead the case of unsteady flow over a circular two dimensional cylinder, since a large body of work exists on the subject, and the mechanism of separation from its curved rear surface appears similar in kind to that occurring at rounded lips. When fluid accelerates from rest, boundary layers develop with time, and their separation from surfaces depends on the duration as well as on the geometry of the flow.

PHILOSOPHICAL TRANSACTIONS OF THE ROYAL SOCIETY A MATHEMATICAL, PHYSICAL & ENGINEERING SCIENCES

Schlichting (1968) describes the case of a circular cylinder which is accelerated from rest in a direction normal to its axis. The time and position of separation are determined by inspection of the velocity gradient at the surface as derived from the pertinent Navier–Stokes equation, since separation is observed to occur following a reversal in polarity of this gradient.

In the circumstances that the acceleration is impulsive, leading to the instantaneous attainment of the final velocity V, the time taken to the moment of separation at its rear stagnation point is given as

$$t_s = 0.096\,R/V, \tag{5.6}$$

where R is the radius of the cylinder; and the distance, S, covered before separation is given as

$$S = 0.351\,R. \tag{5.7}$$

When the acceleration is constant, at a rate b, separation occurs at a time

$$t_s = 1.02\sqrt{(R/b)}, \tag{5.8}$$

after a distance

$$S = 0.52\,R. \tag{5.9}$$

In both cases the distance covered is contingent *only upon the radius of the cylinder*. Hence if the cylinder were to be oscillated back and forth either impulsively or with constant acceleration, the occurrence of separation at some point in the cyle is dependent only upon the oscillation ratio S/R. In the former case, separation occurs when $S/R > 0.35$ and in the latter, when $S/R > 0.52$. Neither form of oscillation is simple harmonic, nor is the reversal of motion included in the theory. However, the ratio S/R may be independently derived by dimensional analysis as an important group in periodic flow and was first shown to characterise lift forces on cylinders in regular waves by Keulegan & Carpenter (1958), who express the number as $U_m\,T/2R$, where U_m is the peak velocity and T is the period of oscillation.

We note that

$$\tfrac{1}{2}U_m\,T/R = \tfrac{1}{2}\pi S/R,$$

where S is the peak-to-peak path length of the motion. ($S = 2\hat{z}$ in simple harmonic motion.)

Many authors have since noted the dependence of separation in periodic flows on the Keulegan–Carpenter number, K_c. Recently Isaacson & Maull (1976) have reported that no separation was observed on a cylinder oscillated in still water for K_c less than 2, and no vortex detachment for K_c less than 4. In addition, they note a relative insensitivity to Reynolds number. A K_c of 2 corresponds to a path length-to-radius ratio of about 1.3, which is of the same order as that derived above from theory. It would certainly appear that, in determining conditions to avoid separation in oscillatory flows, the amplitude ratio S/R is a most important parameter.

Translating these observations to the case of an oscillating duct is clearly not straightforward. However, if a fairly literal interpretation were to be allowed, two immediate conclusions could be drawn: first, that separation and eddy losses will be minimized, and possibly avoided, if the ratio of the flow oscillation amplitude to the radius of curvature of the duct mouth is made small, and secondly, that similarity is dominantly characterized by this ratio which can conveniently be adhered to at any scale of testing since it is satisfied in any geometrically similar model. However, a full analysis of this three dimensional case will probably require an extensive experimental research program.

Frictional damping. The third and final factor to receive attention in this section is fluid friction due to viscosity. We are able to evaluate the contribution of friction to damping losses and also

PHILOSOPHICAL TRANSACTIONS OF THE ROYAL SOCIETY A MATHEMATICAL, PHYSICAL & ENGINEERING SCIENCES

to examine superficially some of the features of the boundary layer within the tube. An exact analysis of the boundary layer would require a solution of the relevant Navier–Stokes equations taking into account the periodicity of the flow, the short length of the tube and the presence of a free surface, all of which serve to complicate the problem to a degree beyond the scope of this investigation. We are again able to make use of certain standard solutions, however, if we first make some simplifying assumptions, namely that we ignore the existence of the free surface and that we consider the inner wall of the tube to be a flat plate (bent into a cylinder), this latter assumption being justified if it can be shown that the thickness of the boundary layer is small compared with the radius of curvature.

The case of laminar periodic flow over an infinitely long flat plate was first solved by Stokes (1851) for a pendulum oscillating in a viscous fluid at rest. If the plate moves in simple harmonic motion in its own plane with velocity

$$V(0, t) = V_0 \cos \omega t, \tag{5.10}$$

the velocity field adjacent to the plate is deduced to be

$$V(y, t) = V_0 \, \mathrm{e}^{-my} \cos(\omega t - my), \tag{5.11}$$

where $m = \sqrt{(\omega/2\nu)}$ and y is the direction normal to the surface. From this it may be seen that a viscous wave extends out from the surface of the plate into the fluid such that the tangential motion of the fluid layers lags progressively behind the motion of the plate, decaying exponentially with distance. The 'wavelength' of the wave normal to the surface is given by $2\pi\sqrt{2\nu/\omega}$, and the thickness of the boundary layer is characteristically of order $\sqrt{(\nu/\omega)}$, which in our experiments is approximately 0.3 mm. (See Lighthill 1978 and Schlichting 1968 for detailed descriptions of this periodic boundary layer in oscillating pipe flow.)

When the plate is held stationary, and the fluid is given a velocity $V_0 \cos \omega t$, the resulting velocity field becomes

$$V(y, t) = V_0 \cos \omega t - V_0 \, \mathrm{e}^{-my} \cos(\omega t - my). \tag{5.12}$$

The shear stress τ_0 on the plate is given by,

$$\tau_0 = \mu \partial V(0, t)/\partial y, \tag{5.13}$$

where μ is the absolute viscosity. Using equations (5.12) and (5.13) the total force applied to a plate of area $2\pi rl$ is given by

$$F = 2\pi r L \mu m V_0 (\cos \omega t - \sin \omega t), \tag{5.14}$$

in which it is noticeable that there is a reactive component in phase with acceleration, contributing here an 'added' mass.

If as before we estimate the energy lost per cycle.

$$E_t = \int_{\text{cycle}} F V_0 \cos \omega t \, \mathrm{d}t. \tag{5.15}$$

Substituting $V_0 = 2\omega$ and using equations (5.15), (5.14), (5.3) and (4.17), we arrive at an expression for the frictional damping ratio:

$$\xi_t = \frac{1}{r}\sqrt{(\nu/2\omega)}. \tag{5.16}$$

Substituting $\omega = \sqrt{(g/L)}$, $r = K_r L$,

$$\xi_t = \nu^{\frac{1}{2}}/K_r \sqrt{2} g^{\frac{1}{4}} L^{\frac{3}{4}}. \tag{5.17}$$

The dimensional dependence of this friction term can be deduced from (5.17), which reveals that friction losses diminish with an increase in linear scale and an increase in tube width ratio K_r. It is of interest to note that frictional damping operates linearly, as assumed for the simulation, since it is derived from a stress that is proportional to velocity.

Substitution of the appropriate experimental values, $K_r = 0.34$, $L = 0.11$, gives

$$\xi_f = 0.006,$$

which is small by most engineering standards, but still just significant in these experiments in relation to the radiation damping term, 0.015.

It may be reasonably assumed from this analysis that friction losses in a practical ocean-scale device will be insignificant unless very narrow tubes are used. An analysis at full scale might, however, require modification to encompass a possible transition to turbulence.

6. Conclusions

It would appear that there are only a certain number of regular periodic eddy geometries to be found in naturally oscillating fluid systems. The Von Karmen vortex streets are probably the most common and have received close examination by other workers. In this paper we have reported two additional stable periodic eddy geometries, namely the jet eddy pair produced by an oscillating flow at the edge of a flat plate, and a periodic vortex ring formation produced by flow in and out of a tube with an abrupt exit. The work reported in this paper on the formation of eddies in unsteady periodic flows complements previous studies on the formation of eddies in steady flows (Berry & Mackley 1977). The generation of eddies represents an area essential to the understanding of turbulence; much emphasis on turbulence studies has been concerned with mechanisms associated with the decay of large eddies to smaller eddies and their subsequent dissipation by viscosity as heat. The mechanisms associated with the generation of initially large eddies has received less attention, where, in terms of the energy extraction of turbulent flows, the controlling factor is the formation of eddies rather than the subsequent dissipation of the energy as the eddies decay. We note in terms of the present work how quickly ordered periodic flows can deteriorate into what visually looks like a form of turbulence; this can be seen both in terms of the behaviour of the jet eddy pairs once they have left the plate and in terms of the transient oscillating response for the abrupt exit tube after about three complete oscillations.

The experiments using resonant ducts have illustrated in a striking manner the effect that eddy formation can have in absorbing energy. When these are combined with our theoretical analysis, we arrive at figures for the 'effective damping ratios' of various contributions. For the example we cite, the radiation damping ratio, ξ_r is of the order 0.015. The friction damping term ξ_f is estimated to be of order 0.005 which is small but possibly significant in comparison to the radiation damping. The eddy damping term ξ_e has two values: when the bell-mouth geometry is used the eddy damping ratio is low and of the order 0.005; when the abrupt exit tube is chosen the eddy damping ratio increases to 0.07 and dominates the process at large amplitudes. We therefore see that eddy motions can be of vital significance to the periodic motions of fluids in and out of ducts.

The observations on the oscillating duct flow have been generalized by establishing approximate relationships on how the various damping ratios change with scale. The radiation damping

ratio is effectively independent of scale and only depends on geometry while the friction damping ratio decreases with increasing scale. The eddy damping ratio, if large, would be expected to remain dominant with increasing scale. However the crucial question is whether experiments that are satisfactorily eddy-free in the laboratory will remain so on an oceanic scale, and if not, how similarity can be ensured. Here we observe through a theoretical approach that a ratio relating the amplitude of motion to the radius of curvature of the duct mouth is of great importance dominating over the Reynolds number at low values when separation is greatly inhibited by time dependent factors. Hence we conclude, with obvious relevance to the design of wave-energy devices, that the behaviour of a model operating with a low value of oscillation amplitude ratio will be essentially similar in any geometrically similar case.

We wish to acknowledge the contribution of Mr D. Carey (Vickers Offshore Ltd) and Professor Sir James Lighthill, F.R.S., whose prior work in this field of wave-energy research largely prompted the present study. We also express our gratitude to our colleagues Dr J. O. Flower and Dr J. M. Owen for helpful discussions during the course of this work, and to Mr K. G. Pike for his skill in making the glass tubes. Finally, we wish to thank the Science Research Council for some financial support and the I.U.I.E.C. for the use of their computer.

References

Batchelor, G. K. 1970 *Fluid dynamics*. Cambridge University Press.
Berry, M. V. & Mackley, M. R. 1977 *Phil. Trans. R. Soc. Lond.* A **287**, 1–16.
Cooper, R. I. B. & Longuet-Higgins, M. S. 1951 *Proc. R. Soc. Lond.* A, **206**, 424–435.
Farley, F., Parks, P. & Altmann, H. 1978 *Proc. International Symposium on Wave and Tidal Energy, BHRA Fluid Engineering*, volume 1, paper No. B2.
Hogben, N., Miller, B., Searle, J. & Ward, G. 1977 *Proc. Instn. civ. Engrs*, part 2, **63** 515–562.
Isaacson, M. & Maull, D. 1976 *J. WatWays Harb. Div. Am. Soc. civ. Engrs.*, **102**, 49–60.
Keulegan, G. H. & Carpenter, L. H. 1958 *J. Res. natn. Bur. Stand*, **60**, 324–440.
Knott, G. F. & Flower, J. O. 1978 *Int. Shipbldg. Prog.* **290**, 257–260.
Knott, G. F. & Flower, J. O. 1979 *J. Fluid Mech.* **90**, 327–336.
Leishman, J. & Scobie, G. 1976 *N. E. L. Report*, nos. EAU M25.
Lighthill, M. J. 1978 *Waves in fluids*, Cambridge University Press.
Lighthill, M. J. 1979 *J. Fluid Mech.* (In the Press).
Longuet-Higgins, M. S. 1977 *Proc. R. Soc. Lond.* A, **352**, 481–503.
Okabe, J. & Inoue, S. 1960 *Rep, Inst. appl. Mech.*, Kyushu Univ. **8**, 91. (Also in Batchelor, 1970).
Popham, E. A. 1949 *The drawings of Leonardo da Vinci*. London: Jonathan Cape.
Prandtl, L. & Tietjens, O. G., 1934 *Applied hydro and aero-mechanics*. New York, Dover.
Sarpkaya, T. 1975 *J. appl. Mechs.* **42**, 32–37.
Schlichting, H. 1968 *Bounday layer theory*. New York: McGraw-Hill.
Stansby, P. K. 1977 *Proc. Instn. civ. Engrs*, part 2, **63**, 865–879.
Stoker, J. J. 1957 *Water waves*. New York: Interscience.
Stokes, G. G. 1851 *Trans. Camb. phil. Soc.* **9**, 8–106.
Ursell, F. 1947 *Proc. Camb. Phil. Soc.* **43**, 374.
Werle, H. 1973 *A. Rev. Fluid Mech.* **5**, 361–382.
Zdravkovich, M. M. 1969 *J. Fluid Mech.* **30**, 491–499.

PHILOSOPHICAL TRANSACTIONS OF THE ROYAL SOCIETY A MATHEMATICAL, PHYSICAL & ENGINEERING SCIENCES

FIGURE 4. Photographs of wave motion interacting with submerged plates. Sequence (*a*)–(*f*) showing development of jet eddy pairs. Wave frequency = 0.83 Hz, wave amplitude = 11 mm. Top of plate 11 cm below surface.

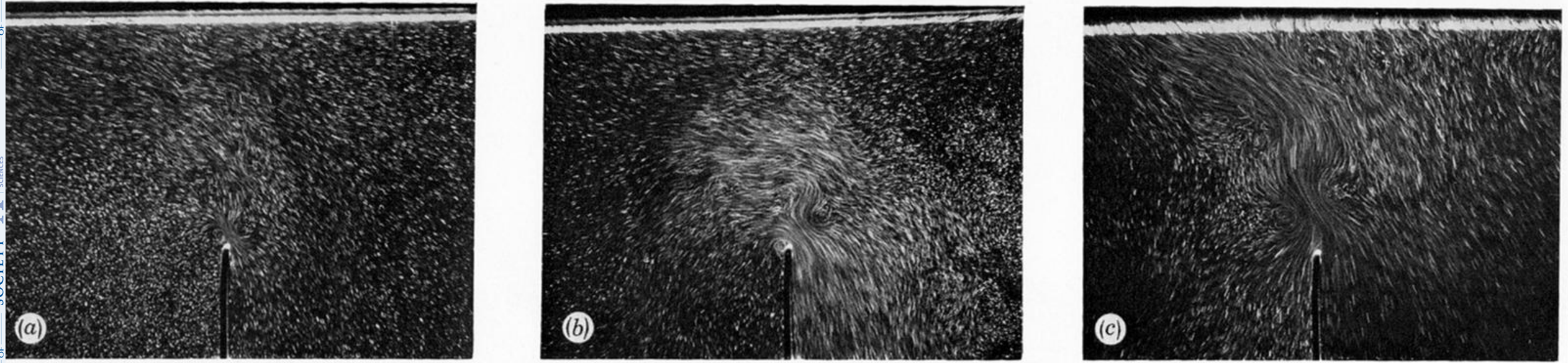

FIGURE 6. Photographic sequence showing the effect of wave amplitude on the intensity of jet eddy pair formation. Wave frequency = 0.83 Hz. Wave amplitude (*a*) = 2 mm, (*b*) = 5 mm, and (*c*) = 11 mm. Other details as figure 4.

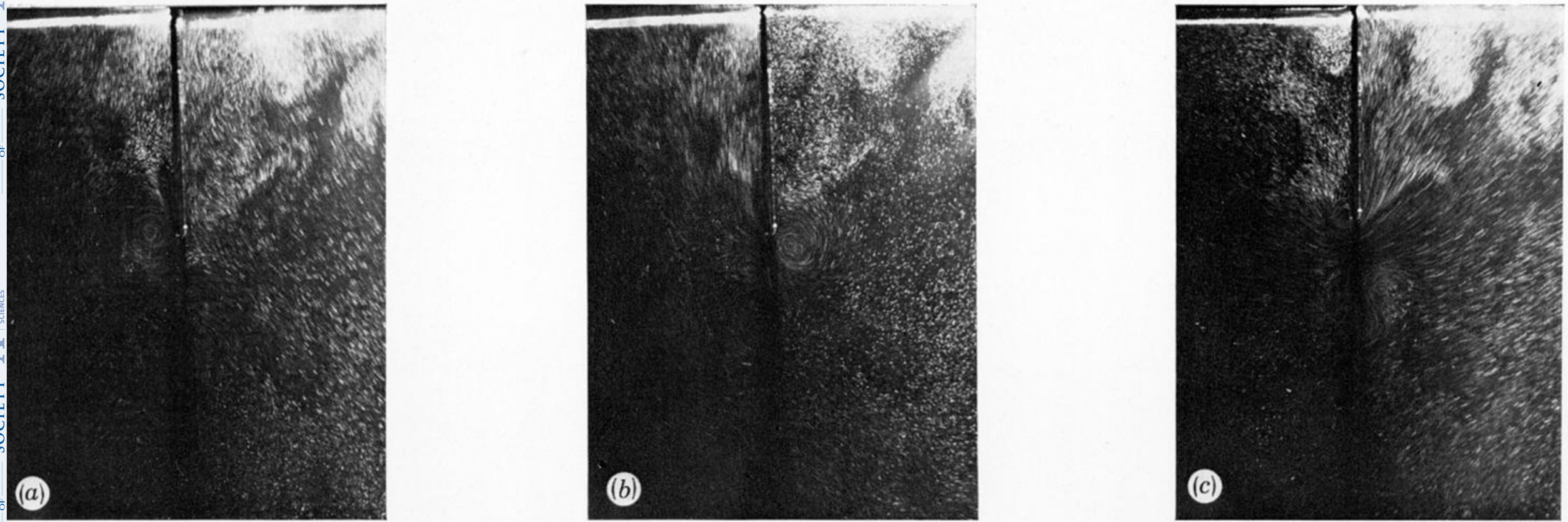

FIGURE 7. Photographic sequence of wave motion interacting with surface piercing plates. Bottom of plate 11 cm below surface. Wave amplitude = 11 mm, wave frequency = 0.83 Hz.

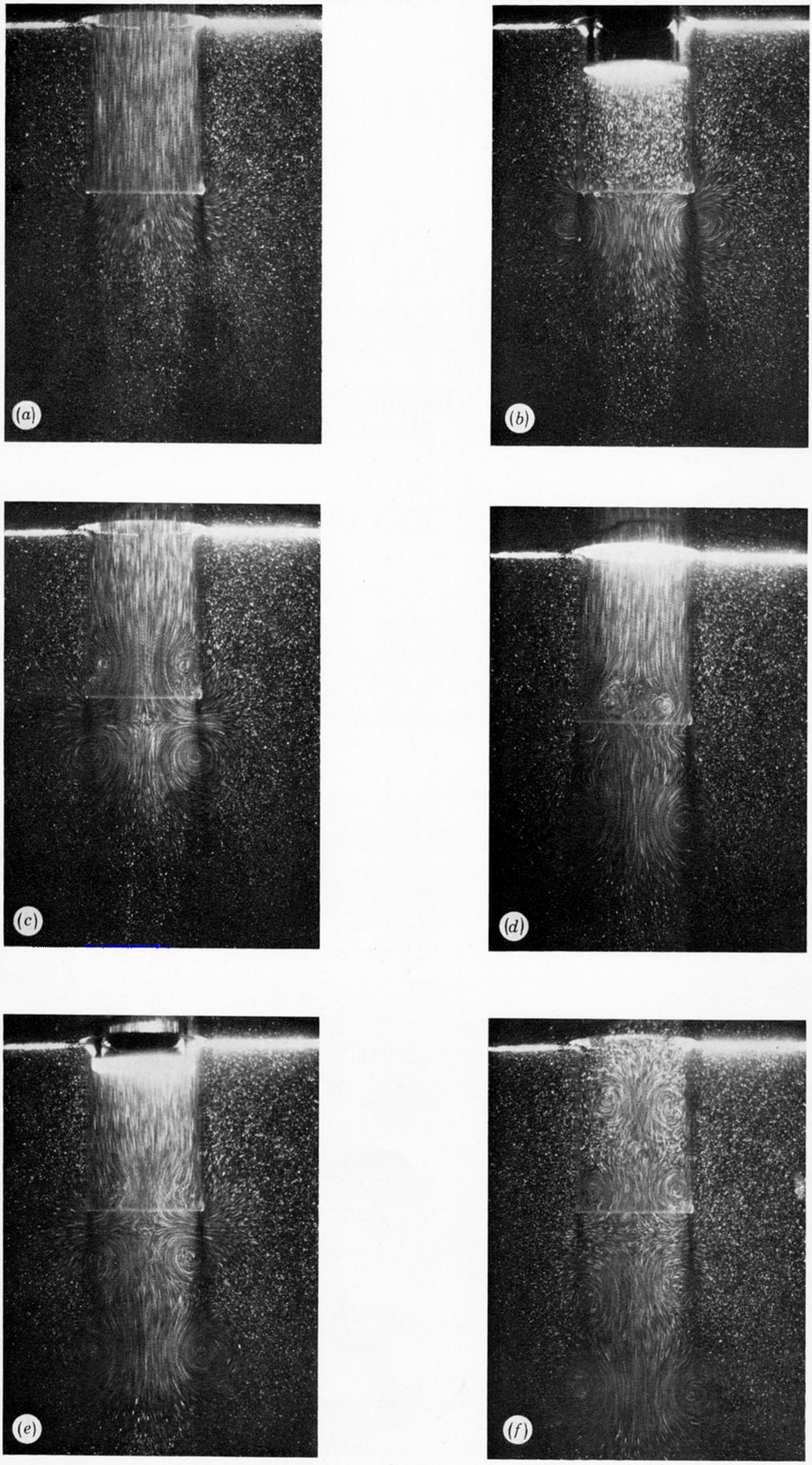

FIGURE 8. Photographic sequence of flow associated with transient response experiment for a parallel-sided tube. Bottom of tube 11 cm below surface. Starting amplitude = 4 cm. Position of each photograph shown in figure 10 *b*.

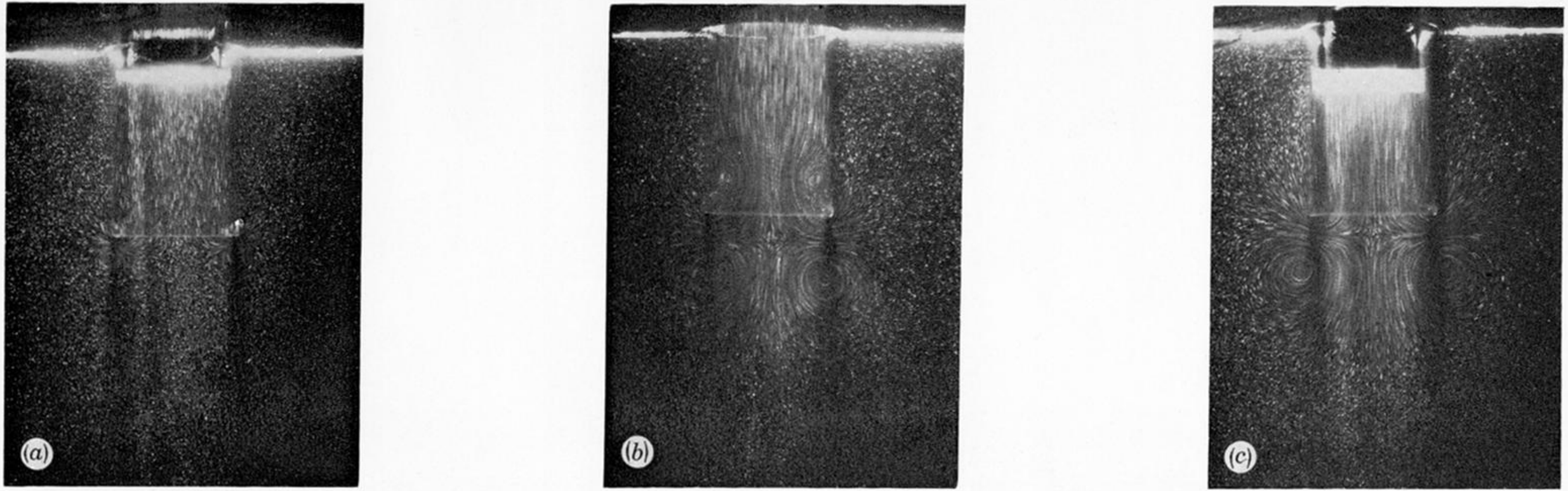

IGURE 11. Photographic sequence showing the effect of starting amplitude on transient response experiments for parallel-sided tube. Starting amplitude $(a) = 2$ cm, $()b = 4$ cm and $(c) = 6$ cm. All photographs taken at approximately bottom of first downward stroke. Other details as figure 8.

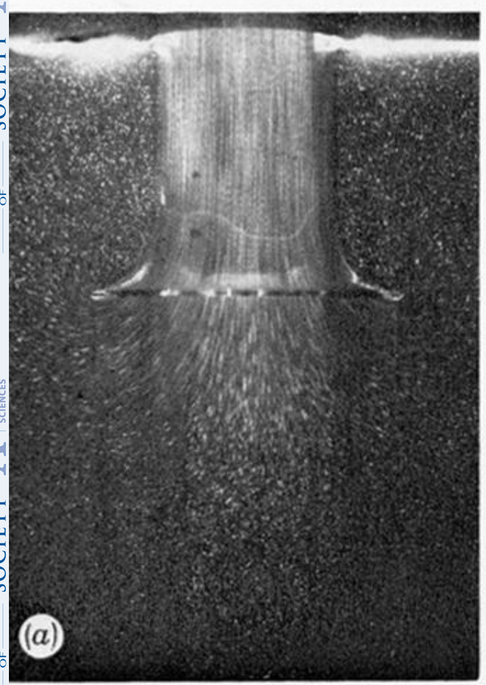

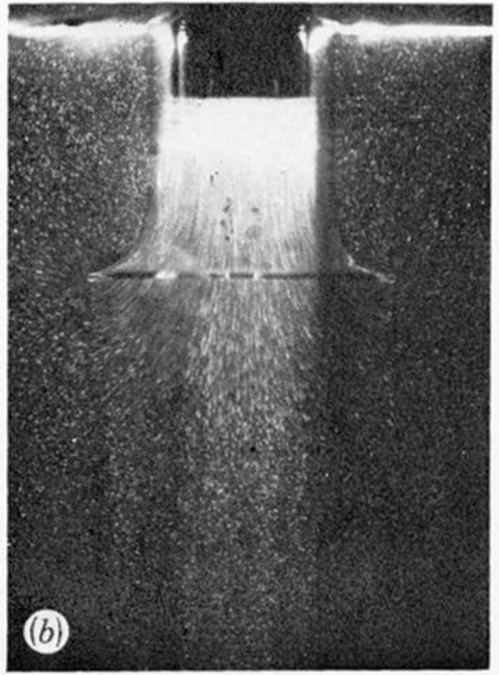

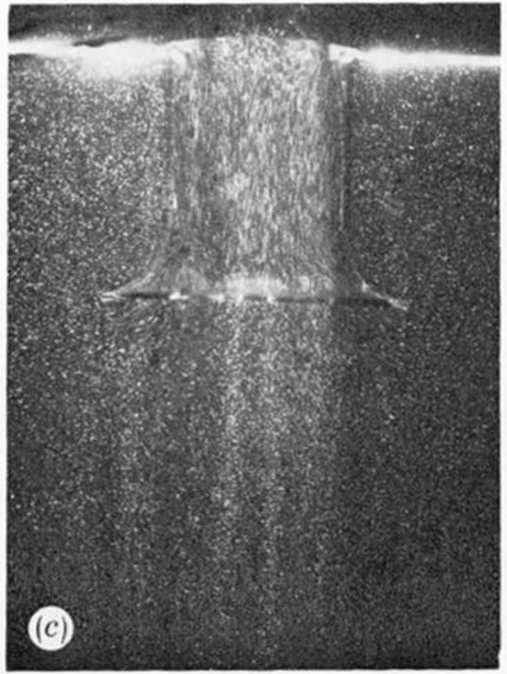

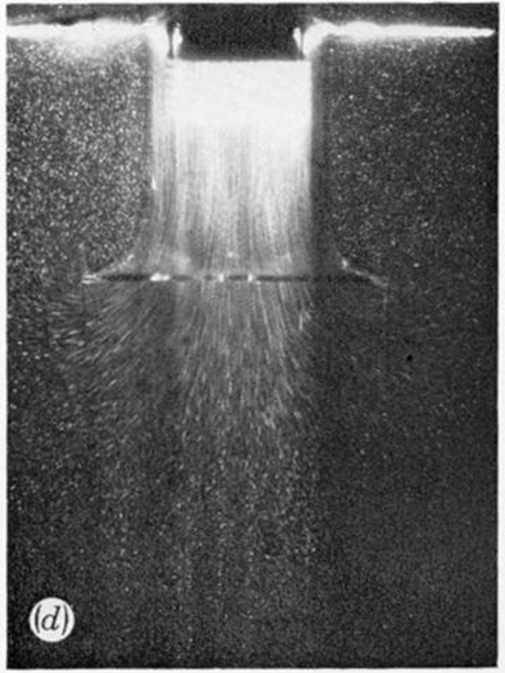

FIGURE 12. Photographic sequence of flows associated with transient response experiment for a bell-mouth tube: bottom of tube 11 cm below surface, Starting amplitude 6 cm, exposure times $\frac{1}{15}$ s. Approximate positions of each photograph shown in figure 13.

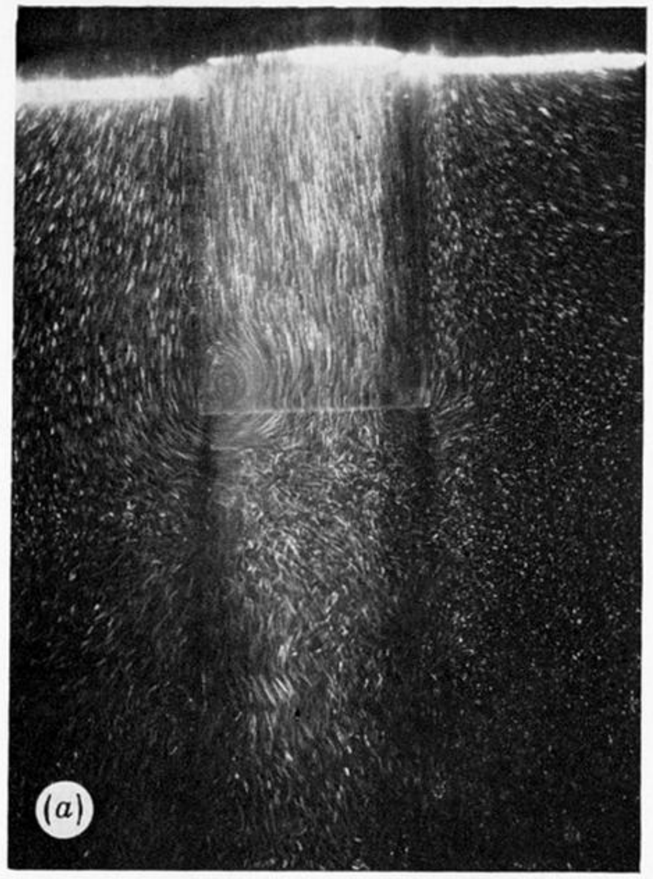

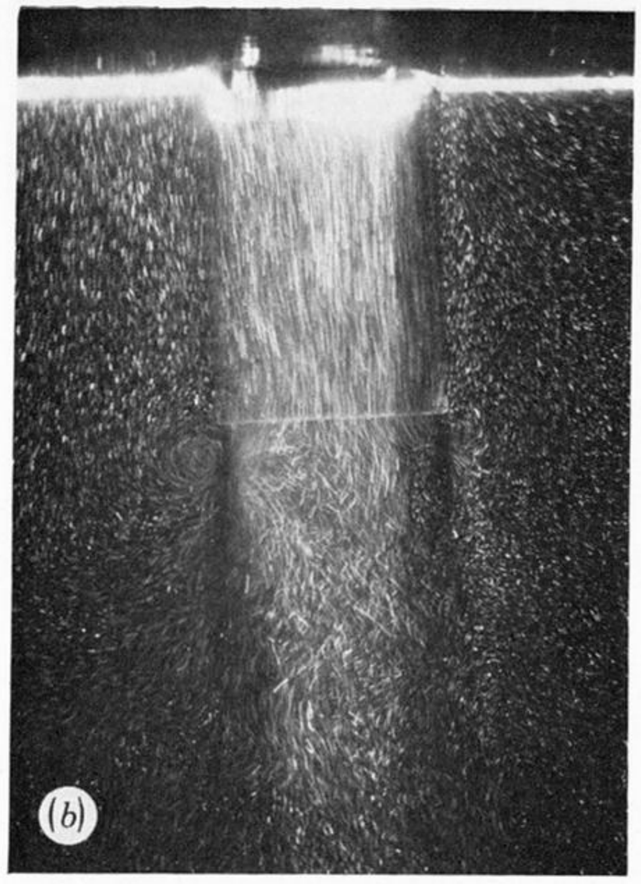

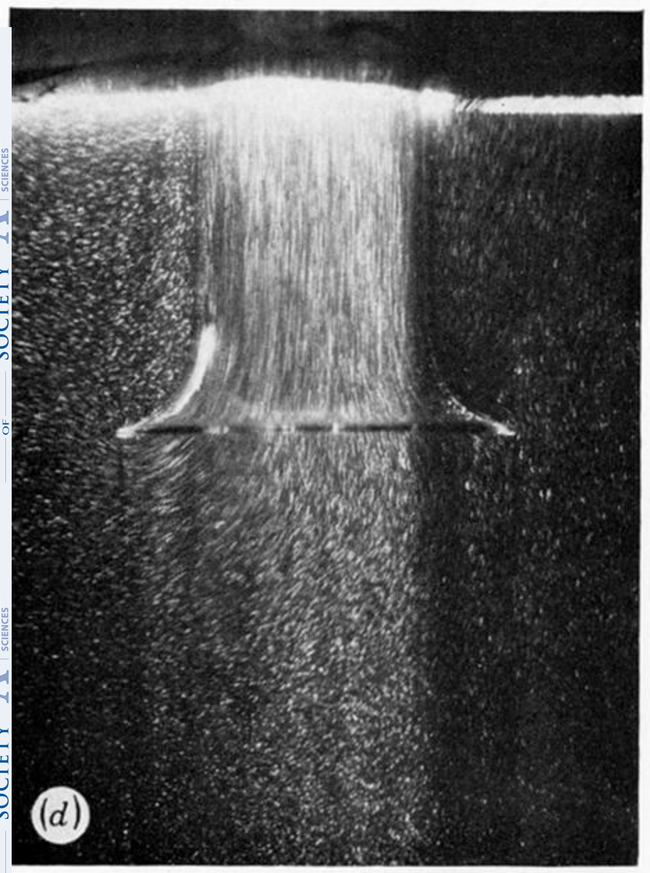

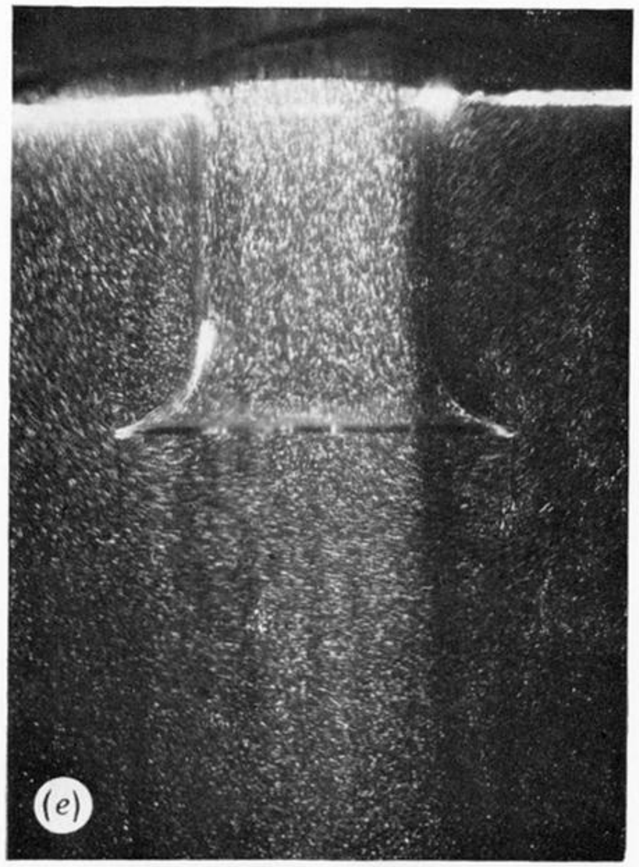

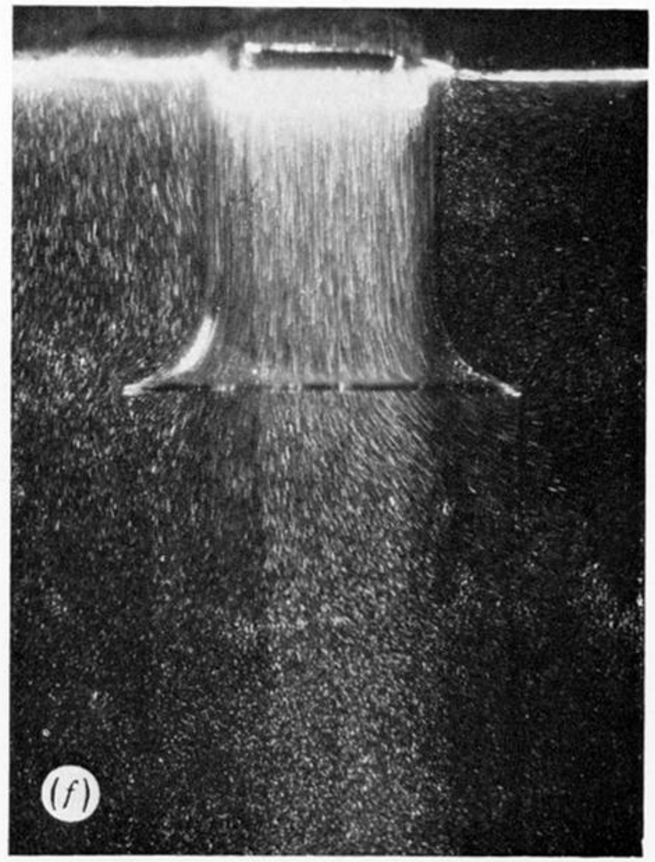

FIGURE 14. Photographic sequence of flows associated with tubes interacting with harmonic waves at different points of wave cycle: wave amplitude = 7 mm, wave frequency = 1.4 Hz, bottom of tubes 11 cm below surface, exposure time = $\frac{1}{8}$ s. Figures 14*a–c*, parallel-sided tube; figures 14*d–f*, bell-mouth tube.

PHILOSOPHICAL TRANSACTIONS OF THE ROYAL SOCIETY A MATHEMATICAL, PHYSICAL & ENGINEERING SCIENCES